Available online at www.sciencedirect.com
ScienceDirect
Comput. Methods Appl. Mech. Engrg. 196 (2007) 2413–2430
Computer methods in applied mechanics and engineering
www.elsevier.com/locate/cma

Time dependent subscales in the stabilized finite element approximation of incompressible flow problems

Ramon Codina [a,*], Javier Principe [a], Oriol Guasch [b], Santiago Badia [a]

[a] Universitat Politècnica de Catalunya, Jordi Girona 1-3, Edifici C1, 08034 Barcelona, Spain
[b] ICR, Enginyeria pel Control del Soroll, Berruguete 52, Vila Olímpica–Vall d'Hebron, 08035 Barcelona, Spain

Received 2 June 2006; received in revised form 26 December 2006; accepted 3 January 2007

Abstract

In this paper we analyze a stabilized finite element approximation for the incompressible Navier–Stokes equations based on the subgrid-scale concept. The essential point is that we explore the properties of the discrete formulation that results allowing the subgrid-scales to depend on time. This apparently "natural" idea avoids several inconsistencies of previous formulations and also opens the door to generalizations.

Keywords: Incompressible flows; Stabilized finite elements; Transient subscales

1. Introduction

Let us start by writing the incompressible Navier–Stokes equations. Consider a domain Ω in $\mathbb{R}^d$, where $d = 2$ or 3 is the number of space dimensions, with boundary $\Gamma = \partial\Omega$, in which we want to solve an incompressible flow problem in the time interval $[0, T]$. If $\boldsymbol{u}$ is the velocity of the fluid and p the pressure, the incompressible Navier–Stokes equations are

$$\partial_t \boldsymbol{u} - \nu\Delta\boldsymbol{u} + \boldsymbol{u}\cdot\nabla\boldsymbol{u} + \nabla p = \boldsymbol{f} \quad \text{in } \Omega,\ t \in]0, T[, \tag{1}$$

$$\nabla\cdot\boldsymbol{u} = 0 \quad \text{in } \Omega,\ t \in]0, T[, \tag{2}$$

where ν is the kinematic viscosity and $\boldsymbol{f}$ is the force vector. These equations must be supplied with an initial condition of the form $\boldsymbol{u} = \boldsymbol{u}^0$ in $\Omega, t = 0$, and a boundary condition which, for simplicity, will be taken as $\boldsymbol{u} = \boldsymbol{0}$ on $\Gamma, t \in]0, T[$.

Let us introduce some standard notation. The space of functions whose p power ($1 \leqslant p < \infty$) is integrable in a domain Ω is denoted by $L^p(\omega)$, $L^\infty(\omega)$ being the space of bounded functions in Ω. The space of functions whose distributional derivatives of order up to $m \geqslant 0$ (integer) belong to $L^2(\omega)$ is denoted by $H^m(\omega)$. The space $H^1_0(\omega)$ consists of functions in $H^1(\omega)$ vanishing on $\partial\omega$. The topological dual of $H^1_0(\omega)$ is denoted by $H^{-1}(\omega)$. A bold character is used to denote the vector counterpart of all these spaces.

If f and g are functions (or distributions) such that fg is integrable in the domain ω under consideration, we denote

$$\langle f, g\rangle_\omega = \int_\omega fg\,\mathrm{d}\omega,$$

so that, in particular, $\langle\cdot,\cdot\rangle_\omega$ is the duality pairing between $H^{-1}(\omega)$ and $H^1_0(\omega)$. When $f, g \in L^2(\omega)$, we write the inner product as $\langle f, g\rangle_\omega \equiv (f, g)_\omega$. The norm in a Banach space X is denoted by $\|\cdot\|_X$, and $L^p(0, T; X)$ is the space of time dependent functions such that their X-norm is $L^p(0, T)$. This notation is simplified in some cases as follows: $(\cdot,\cdot)_\Omega \equiv (\cdot,\cdot)$, $\langle\cdot,\cdot\rangle_\Omega \equiv \langle\cdot,\cdot\rangle$ and $\|\cdot\|_{L^2(\Omega)} \equiv \|\cdot\|$.

Using this notation, the velocity and pressure finite element spaces for the continuous problem are $\boldsymbol{L}^2(0, T; \mathscr{V}^d_0)$ and $L^1(0, T; \mathscr{Q}_0)$ (for example), respectively, where $\mathscr{V}^d_0 := \boldsymbol{H}^1_0(\Omega)$, $\mathscr{Q}_0 := L^2(\Omega)/\mathbb{R}$. The weak form of the problem consists in finding $[\boldsymbol{u}, p] \in \boldsymbol{L}^2(0, T; \mathscr{V}^d_0) \times L^1(0, T; \mathscr{Q}_0)$ such that

* Corresponding author.
E-mail addresses: ramon.codina@upc.edu (R. Codina), principe@cimne.upc.edu (J. Principe), oguasch@icrsl.com (O. Guasch), sbadia@cimne.upc.edu (S. Badia).

0045-7825/$ - see front matter © 2007 Elsevier B.V. All rights reserved.
doi:10.1016/j.cma.2007.01.002

$$(\partial_t \boldsymbol{u}, \boldsymbol{v}) + \nu(\nabla \boldsymbol{u}, \nabla \boldsymbol{v}) + \langle \boldsymbol{u} \cdot \nabla \boldsymbol{u}, \boldsymbol{v} \rangle - (p, \nabla \cdot \boldsymbol{v}) = \langle \boldsymbol{f}, \boldsymbol{v} \rangle, \quad (3)$$

$$(q, \nabla \cdot \boldsymbol{u}) = 0 \quad (4)$$

for all $[\boldsymbol{v}, q] \in \mathcal{V}_0^d \times \mathcal{Q}_0$, and satisfying the initial condition in a weak sense.

The Galerkin finite element approximation of problem (3), (4) consists in seeking the unknowns in finite dimensional spaces $\mathcal{V}_{0,h}^d \subset \mathcal{V}_0^d$ and $\mathcal{Q}_{0,h} \subset \mathcal{Q}_0$ and taking the test functions also in these spaces. Using the method of lines, the problem discretized in space, but still continuous in time, consists in finding $[\boldsymbol{u}_h(t), p_h(t)] \in \boldsymbol{L}^2(0, T; \mathcal{V}_{0,h}^d) \times L^1(0, T; \mathcal{Q}_{0,h})$ such that

$$(\partial_t \boldsymbol{u}_h, \boldsymbol{v}_h) + \nu(\nabla \boldsymbol{u}_h, \nabla \boldsymbol{v}_h) + \langle \boldsymbol{u}_h \cdot \nabla \boldsymbol{u}_h, \boldsymbol{v}_h \rangle - (p_h, \nabla \cdot \boldsymbol{v}_h) = \langle \boldsymbol{f}, \boldsymbol{v}_h \rangle, \quad (5)$$

$$(q_h, \nabla \cdot \boldsymbol{u}_h) = 0 \quad (6)$$

for all $[\boldsymbol{v}_h, q_h] \in \mathcal{V}_{0,h}^d \times \mathcal{Q}_{0,h}$.

Once discretized in time (using for example a finite difference scheme), it is well known that problem (5), (6) suffers from different types of numerical instabilities. Two of them are inherited from the stationary problem, namely, the dominance of the (nonlinear) convective term over the viscous one when ν is small and the compatibility required for the velocity and pressure finite element spaces posed by the inf–sup condition. There are also numerical instabilities encountered when the time step size of the time discretization is small, particularly in early stages of the time integration.

A vast literature exists dealing with the instabilities due to the dominance of convection and to the velocity–pressure compatibility condition. In this work we adopt a *stabilized* finite element formulation based on the subgrid-scale concept and, in particular, in the approach introduced by Hughes in [24,26] for the scalar convection–diffusion equation. The basic idea is to approximate the *effect* of the component of the continuous solution which cannot be resolved by the finite element mesh, which we will call *subscale*, on the discrete finite element solution. This approach is a general framework in which it is possible to design different stabilized formulations. We will restrict our attention to two approaches, described in [10,11]. In the first case, the velocity and pressure subscales are taken proportional to the residual of the finite element component in the momentum and in the continuity equations, respectively. The bottom line of the second approach is to take only the component of these residuals L^2 orthogonal to the finite element space. This idea was first introduced in [8] as an extension of a stabilization method originally introduced for the Stokes problem in [12] and fully analyzed for the stationary Navier–Stokes equations in [13].

However, the main interest of this paper is *not* how to stabilize convection-dominated flows or how to be able to use equal velocity–pressure interpolation, thus avoiding the need to satisfy the inf–sup condition that problem (5), (6) demands. Our objective in this paper is *to analyze the formulation that stems from considering time dependent subscales*. In fact, the idea we will follow is not new, and was already introduced in [11]. In this sense, the present work can be considered as a continuation of this reference, with the emphasis placed solely on the consequences of taking the subscales time dependent. We contribute here with the study of several properties of the formulation, including an analysis of its stability and more numerical experiments to check its performance.

The paper is organized as follows. The numerical formulation is described in Section 2, and its main features and its stability analysis are presented in Sections 3 and 4, respectively. In the former, we detail the benefits of considering the subscales time dependent, and how some of the misbehaviors of classical stabilized finite element methods are overcome. We also end Section 3 with a speculative subsection considering the tracking of subscales along the nonlinear process as a way to model turbulence. This idea was also pointed out in [11]. The stability analysis of Section 4 is done for the *linearized* problem, that is, replacing the advection velocity $\boldsymbol{u}$ by a known velocity $\boldsymbol{a}$, which is assumed to be constant. In spite of this simplification, this stability analysis allows us to highlight the improvement in the stability of the original Galerkin formulation (5), (6) introduced by the time dependent subscales. In Section 5 we present the results of three simple numerical examples that show the benefits of our approach. The paper concludes with some final remarks in Section 6.

2. Stabilized finite element problem

Let us consider a finite element partition of the domain Ω with n_{el} elements. A generic element domain will be denoted by K and its diameter by h_K. To simplify the discussion, we will consider quasi-uniform finite element partitions, so that if $h = \max_K h_K$ and $\varrho = \min_K \varrho_K$, with ϱ_K the diameter of the ball inscribed in K, the quotient h/ϱ remains bounded for all partitions. Likewise, we will assume that *all the finite element spaces constructed are continuous* and of the same order for the velocity and the pressure.

The starting idea of the formulation we propose is the variational multiscale formulation proposed in [24,26]. Let $\mathcal{V}_0^d = \mathcal{V}_{0,h}^d \oplus \widetilde{\mathcal{V}}_0^d$, where $\mathcal{V}_{0,h}^d$ is the velocity finite element space and $\widetilde{\mathcal{V}}_0^d$ any space to complete $\mathcal{V}_{0,h}^d$ in $\mathcal{V}_0^d$. Similarly, let $\mathcal{Q}_0 = \mathcal{Q}_{0,h} \oplus \widetilde{\mathcal{Q}}_0$. The original continuous problem (3), (4) is equivalent to find $[\boldsymbol{u}_h(t), p_h(t)] \in \boldsymbol{L}^2(0, T; \mathcal{V}_{0,h}^d) \times L^1(0, T; \mathcal{Q}_{0,h})$, as well as $[\tilde{\boldsymbol{u}}(t), \tilde{p}(t)] \in \boldsymbol{L}^2(0, T; \widetilde{\mathcal{V}}_0^d) \times L^1(0, T; \widetilde{\mathcal{Q}}_0)$, such that

$$(\partial_t(\boldsymbol{u}_h + \tilde{\boldsymbol{u}}), \boldsymbol{v}) + \nu(\nabla(\boldsymbol{u}_h + \tilde{\boldsymbol{u}}), \nabla \boldsymbol{v}) + \langle (\boldsymbol{u}_h + \tilde{\boldsymbol{u}}) \cdot \nabla(\boldsymbol{u}_h + \tilde{\boldsymbol{u}}), \boldsymbol{v} \rangle - (p_h + \tilde{p}, \nabla \cdot \boldsymbol{v}) = \langle \boldsymbol{f}, \boldsymbol{v} \rangle, \quad (7)$$

$$(q, \nabla \cdot (\boldsymbol{u}_h + \tilde{\boldsymbol{u}})) = 0 \quad (8)$$

for all $[\boldsymbol{v}, q] \in \mathcal{V}_0^d \times \mathcal{Q}_0$. These equations can be split into two systems by taking first $[\boldsymbol{v}, q] = [\boldsymbol{v}_h, q_h] \in \mathcal{V}_{0,h}^d \times \mathcal{Q}_{0,h}$ and then $[\boldsymbol{v}, q] = [\tilde{\boldsymbol{v}}, \tilde{q}] \in \widetilde{\mathcal{V}}_0^d \times \widetilde{\mathcal{Q}}_0$. Denoting by $\boldsymbol{n}$ the

exterior unit normal to an integration domain, after integrating some terms by parts the first choice leads to

$$(\partial_t(\boldsymbol{u}_h+\tilde{\boldsymbol{u}}),\boldsymbol{v}_h)+\nu(\nabla\boldsymbol{u}_h,\nabla\boldsymbol{v}_h)+\nu\sum_K[-(\tilde{\boldsymbol{u}},\Delta\boldsymbol{v}_h)_K+\langle\tilde{\boldsymbol{u}},\boldsymbol{n}\cdot\nabla\boldsymbol{v}_h\rangle_{\partial K}]+\langle(\boldsymbol{u}_h+\tilde{\boldsymbol{u}})\cdot\nabla\boldsymbol{u}_h,\boldsymbol{v}_h\rangle-\langle\tilde{\boldsymbol{u}},(\boldsymbol{u}_h+\tilde{\boldsymbol{u}})\cdot\nabla\boldsymbol{v}_h\rangle-(p_h+\tilde{p},\nabla\cdot\boldsymbol{v}_h)=\langle\boldsymbol{f},\boldsymbol{v}_h\rangle, \tag{9}$$

$$(q_h,\nabla\cdot\boldsymbol{u}_h)-(\nabla q_h,\tilde{\boldsymbol{u}})=0, \tag{10}$$

where we have used the fact that $\nabla\cdot(\boldsymbol{u}_h+\tilde{\boldsymbol{u}})=0$, that the sum of the integral of $\boldsymbol{n}\cdot(\boldsymbol{u}_h+\tilde{\boldsymbol{u}})$ on the boundaries of two adjacent elements (and thus with opposite normals $\boldsymbol{n}$) must be zero and that $\boldsymbol{u}_h=\tilde{\boldsymbol{u}}=\boldsymbol{0}$ on Γ.

The second system is obtained by taking $[\boldsymbol{v},q]=[\tilde{\boldsymbol{v}},\tilde{q}]\in\widetilde{\mathscr{V}}_0^d\times\widetilde{\mathscr{Q}}_0$ in (7), (8). Of course, the resulting system, together with (9), (10), is exactly equivalent to (3), (4). A *stabilized finite element method* is obtained if $\tilde{\boldsymbol{u}}$ and $\tilde{p}$ *are approximated* and their expression inserted into (9), (10).

It is not our purpose in this paper to emphasize how to obtain the approximations for $\tilde{\boldsymbol{u}}$ and $\tilde{p}$, but

- To allow $\tilde{\boldsymbol{u}}$ to be time dependent, and therefore to keep its time dependency in (9).
- To note that the advection velocity in (9) is $\boldsymbol{u}_h+\tilde{\boldsymbol{u}}$, and not only $\boldsymbol{u}_h$.

In fact, we will not explore in detail the second item. Some comments about this point will be made later on. Our main concern will be to study the properties of the numerical formulation that emanates from considering $\tilde{\boldsymbol{u}}$ time dependent. For this purpose, it is enough to make some simplifying assumptions:

- The term involving integrals over interelement boundaries will be neglected. This can be understood as considering the velocity subscales as bubble functions, vanishing on the boundaries of the elements (see, e.g., [1,4]). Even though its consideration can bring important stabilization properties, it is not essential for what follows.
- The approximation of the subgrid-scales is performed as follows. The system for the subscales $[\tilde{\boldsymbol{u}}(t),\tilde{p}(t)]$, obtained taking $[\boldsymbol{v},q]=[\tilde{\boldsymbol{v}},\tilde{q}]\in\widetilde{\mathscr{V}}_0^d\times\widetilde{\mathscr{Q}}_0$, can be understood as

$$\partial_t\tilde{\boldsymbol{u}}+(\boldsymbol{u}_h+\tilde{\boldsymbol{u}})\cdot\nabla\tilde{\boldsymbol{u}}-\nu\Delta\tilde{\boldsymbol{u}}+\nabla\tilde{p}=\boldsymbol{r}_{u,h},$$
$$\nabla\cdot\tilde{\boldsymbol{u}}=r_{p,h},$$

where $\boldsymbol{r}_{u,h}$ and $r_{p,h}$ are appropriate residuals of the finite element components $\boldsymbol{u}_h$ and p_h adequately projected onto the space of subscales ($\widetilde{\mathscr{V}}_0^d$ for the first equation and $\widetilde{\mathscr{Q}}_0$ for the second). Using for example the arguments described in [11], based on a Fourier analysis of the problem for the subscales, the following approximation to the previous equations can be motivated:

$$\partial_t\tilde{\boldsymbol{u}}+\frac{1}{\tau_1}\tilde{\boldsymbol{u}}=\boldsymbol{r}_{u,h}, \tag{11}$$

$$\frac{1}{\tau_2}\tilde{p}=r_{p,h}+\tau_1\partial_t r_{p,h}, \tag{12}$$

where

$$\tau_1=\left[c_1\frac{\nu}{h^2}+c_2\frac{|\boldsymbol{u}_h+\tilde{\boldsymbol{u}}|}{h}\right]^{-1}, \tag{13}$$

$$\tau_2=\frac{h^2}{c_1\tau_1}, \tag{14}$$

$$\boldsymbol{r}_{u,h}=-\mathscr{P}[\partial_t\boldsymbol{u}_h+(\boldsymbol{u}_h+\tilde{\boldsymbol{u}})\cdot\nabla\boldsymbol{u}_h-\nu\Delta\boldsymbol{u}_h+\nabla p_h-\boldsymbol{f}], \tag{15}$$

$$r_{p,h}=-\mathscr{P}[\nabla\cdot\boldsymbol{u}_h]. \tag{16}$$

In these expressions, c_1 and c_2 are algorithmic parameters (of order 1) and $\mathscr{P}$ can be either the identity for "classical" stabilized finite element methods (which can be traced back to [5], for example) or the projection orthogonal to the finite element space (we have used the same symbol for the scalar and vector counterparts of this operator). As in [10,11] we will refer to the choice $\mathscr{P}=I$ (identity) as the Algebraic Subgrid-Scale formulation (ASGS), whereas $\mathscr{P}=\Pi_h^{\perp}$, Π_h being the L^2 projection onto the appropriate finite element space (of velocities or of pressures), will lead to the so-called Orthogonal Subscales Stabilization (OSS).

As is shown in [28], the fine-scale component of the solution is related to the residual of the coarse scales through so-called small-scale Green's function. It was also shown in [28] that the small-scale Green's function is highly localized for the right choice of the projector, rendering local algebraic approximations (11), (12) a viable model for the fine scales.

Again, let us stress that the two assumptions described are not essential for our discussion and could be modified. The important point is that $\partial_t\tilde{\boldsymbol{u}}$ appears in the *approximate* equation for the velocity subscale. In our case, this approximation turns out to be the differential equation in time (11).

Remark 1. Observe that Eq. (11) must hold at each point, and therefore it is in fact an *ordinary differential equation* rather than a partial differential equation.

Remark 2. Neglecting the time derivative in (11) could be understood as considering that the subscales adapt automatically to the finite element residual. The subscales obtained from this assumption were defined in [11] as *quasi-static*.

Remark 3. Observe that (11) is a nonlinear equation, due to the dependence of τ_1 and $\boldsymbol{r}_{u,h}$ on $\tilde{\boldsymbol{u}}$. Obviously, this does not depend on whether the subscales vary in time or not, and was also noticed in [7] for what we have called quasi-static subscales. In this case, it is possible to tackle directly the resulting nonlinear *algebraic* equation and solve for $\tilde{\boldsymbol{u}}$ in terms of $\boldsymbol{r}_{u,h}$ accounting for this nonlinearity.

However, in our case this is not possible, and we will have to linearize (11) to integrate it in time.

Remark 4. The approximation for the pressure subscale (12) comes from taking the divergence of the momentum equation, using the continuity equation and then approximating the resulting pressure Poisson equation. Following this procedure, the second term in the right-hand-side of this equation appears naturally. In some situations, we have found it crucial to improve pressure stability.

The formulation we want to analyze is now complete. It consists of solving (9), (10) *together with* (11), (12) for $\boldsymbol{u}_h$, $\tilde{\boldsymbol{u}}$, p_h and $\tilde{p}$, neglecting the integrals over interelements boundaries, as it has been mentioned. Although it does not introduce any particular complication, as it can be observed from the analysis in [10,11], we will take $\tilde{p}=0$ for the sake of simplicity (in fact, we have used expression (12) with τ_2 given by (14) in the numerical examples of Section 5). Therefore, the final problem we have to solve can be written as a single variational equation as follows: find $[\boldsymbol{u}_h(t), p_h(t)] \in \boldsymbol{L}^2(0,T;\mathscr{V}^d_{0,h}) \times L^1(0,T;\mathscr{Q}_{0,h})$ such that

$$\begin{aligned}&(\partial_t \boldsymbol{u}_h, \boldsymbol{v}_h) + \nu(\nabla \boldsymbol{u}_h, \nabla \boldsymbol{v}_h) + \langle \boldsymbol{u}_h \cdot \nabla \boldsymbol{u}_h, \boldsymbol{v}_h\rangle - (p_h, \nabla\cdot \boldsymbol{v}_h)\\ &\quad + (q_h, \nabla\cdot \boldsymbol{u}_h) - \langle \boldsymbol{v}_h, \boldsymbol{f}\rangle + (\partial_t \tilde{\boldsymbol{u}}, \boldsymbol{v}_h) + \langle \tilde{\boldsymbol{u}}\cdot\nabla \boldsymbol{u}_h, \boldsymbol{v}_h\rangle\\ &\quad - \langle \tilde{\boldsymbol{u}}, \tilde{\boldsymbol{u}}\cdot\nabla \boldsymbol{v}_h\rangle - \sum_K \langle \tilde{\boldsymbol{u}}, \nu\Delta \boldsymbol{v}_h + \boldsymbol{u}_h\cdot\nabla \boldsymbol{v}_h + \nabla q_h\rangle_K = 0\end{aligned} \tag{17}$$

for all $[\boldsymbol{v}_h, q_h] \in \mathscr{V}^d_{0,h} \times \mathscr{Q}_{0,h}$, where $\tilde{\boldsymbol{u}}$ is solution of the nonlinear differential equation (11), with τ_1 given by (13) and $\boldsymbol{r}_{u,h}$ by (15). In what follows, we will rename $\tau_1 \equiv \tau$.

Remark 5. From the point of view of the implementation of the method, it is clear from (17) that $\tilde{\boldsymbol{u}}$ is needed at the numerical integration points within each element. Therefore, (11) has to be integrated in time at each integration point. In this sense, $\tilde{\boldsymbol{u}}$ acts as what would be called *internal variable* in solid mechanics.

Remark 6. If the subscales are assumed to be orthogonal to the finite element space, the term $(\partial_t \tilde{\boldsymbol{u}}, \boldsymbol{v}_h)$ vanishes and, as explained in [11], the term $\sum_K \langle \tilde{\boldsymbol{u}}, \nu\Delta \boldsymbol{v}_h + \boldsymbol{u}_h\cdot\nabla \boldsymbol{v}_h + \nabla q_h\rangle_K$ can be replaced by $\sum_K \langle \tilde{\boldsymbol{u}}, \boldsymbol{u}_h\cdot\nabla \boldsymbol{v}_h + \nabla q_h\rangle_K$ and still keep the same accuracy of the method.

Remark 7. Problem (9)–(12) needs to be completed with initial conditions $\boldsymbol{u}_h = \boldsymbol{u}_h^0$ and $\tilde{\boldsymbol{u}} = \tilde{\boldsymbol{u}}^0$ at $t=0$, where the functions $\boldsymbol{u}_h^0$ and $\tilde{\boldsymbol{u}}^0$ depend on the way to choose the space of subscales. We assume that the projections onto the finite element space and the space of subscales are L^2 continuous (this is obvious if $\mathscr{P} = \Pi_h^+$ in (15)), and therefore $\|\boldsymbol{u}_h^0\| \leqslant C\|\boldsymbol{u}^0\|$, $\|\tilde{\boldsymbol{u}}^0\| \leqslant C\|\boldsymbol{u}^0\|$ for a certain constant C.

3. Main features of the formulation

The left-hand-side of the discrete variational form of the problem given by (17) consists of the following terms:

$$(\partial_t \boldsymbol{u}_h, \boldsymbol{v}_h) + \nu(\nabla \boldsymbol{u}_h, \nabla \boldsymbol{v}_h) + \langle \boldsymbol{u}_h\cdot\nabla \boldsymbol{u}_h, \boldsymbol{v}_h\rangle - (p_h, \nabla\cdot \boldsymbol{v}_h) + (q_h, \nabla\cdot \boldsymbol{u}_h) - \langle \boldsymbol{v}_h, \boldsymbol{f}\rangle \quad \text{Galerkin terms,} \tag{18}$$

$$-\sum_K \langle \tilde{\boldsymbol{u}}, \nu\Delta \boldsymbol{v}_h + \boldsymbol{u}_h\cdot\nabla \boldsymbol{v}_h + \nabla q_h\rangle_K \quad \text{Stabilization terms,} \tag{19}$$

$$(\partial_t \tilde{\boldsymbol{u}}, \boldsymbol{v}_h) + \langle \tilde{\boldsymbol{u}}\cdot\nabla \boldsymbol{u}_h, \boldsymbol{v}_h\rangle - \langle \tilde{\boldsymbol{u}}, \tilde{\boldsymbol{u}}\cdot\nabla \boldsymbol{v}_h\rangle \quad \text{Effect of } \tilde{\boldsymbol{u}} \text{ in the material derivative.} \tag{20}$$

The stabilization terms appear also in the stationary and linearized problem, and it is now well known that they allow to overcome the instability problems of the classical Galerkin formulation, which in this case are the instabilities found in convection-dominated flows and the need to satisfy an inf–sup condition for the velocity and pressure interpolations.

The terms associated to the effect of $\tilde{\boldsymbol{u}}$ in the material derivative are precisely those that come from accepting the decomposition $\boldsymbol{u}_h + \tilde{\boldsymbol{u}}$ in the expression of

$$\begin{aligned}\frac{\mathrm{D}}{\mathrm{D}t}\boldsymbol{u} &= \frac{\mathrm{D}}{\mathrm{D}t}(\boldsymbol{u}_h + \tilde{\boldsymbol{u}})\\ &= \partial_t \boldsymbol{u}_h + \partial_t \tilde{\boldsymbol{u}} + \tilde{\boldsymbol{u}}\cdot\nabla \boldsymbol{u}_h + \boldsymbol{u}_h\cdot\nabla \boldsymbol{u}_h + \tilde{\boldsymbol{u}}\cdot\nabla \tilde{\boldsymbol{u}} + \boldsymbol{u}_h\cdot\nabla \tilde{\boldsymbol{u}}.\end{aligned} \tag{21}$$

Only the last of these terms where $\tilde{\boldsymbol{u}}$ appears contributes to the stabilization terms. Our objective is to discuss precisely the effect of the other terms contributed by $\tilde{\boldsymbol{u}}$.

3.1. Commutation of space and time discretization

Let us start our discussion on the properties of the method just presented by noting that we have been able to formulate a *stabilized finite element method* without any reference to the time discretization. Usually, the problem of formulating stabilized methods for time dependent problems has been tackled using two main approaches:

- By using space–time finite element formulations, and considering the temporal derivative in the same way as the first order spatial derivatives of the convective term. This is the approach adopted for example in the early papers on this subject [33,36].
- By discretizing first in time, and then using a stabilized finite element method for the resulting spatially continuous problem. This is perhaps the most popular approach in the literature. The design of the time integration scheme is in principle independent of the stabilization formulation used, but can be adapted to improve the behavior in time of the solution (see, e.g., [32]).

Space time formulations of order higher than one require predictor–corrector strategies to avoid an unacceptable increase in the number of unknowns treated at once (see, e.g., [36]). On the other hand, first order methods, with piecewise constant interpolations in time, lead to very poor schemes, that need to be modified *a posteriori* to

improve their accuracy [31]. In particular, it turns out to be essential to include an approximation of the time derivative in the residual given by (15). This comes out naturally if the equations are first discretized in time using a finite difference scheme.

Nevertheless, in the subgrid-scale formulation we are analyzing, the fact of considering the subscales time dependent allows us either to start from the time discrete problem, as in [11], or to use a method of lines, discretizing first in space and then in time, which is the approach we are following here. Both methods *will lead exactly to the same fully discrete scheme, that is to say, space and time discretization commute*, even when using finite difference schemes in time. In general, this property is trivial only for stabilized methods that do not involve the residual of the equations to be solved, as the method proposed in [6] or even the stabilization with quasi-static orthogonal subscales [11]. However, in this case stability estimates can be obtained assuming a certain dependence of the stabilization parameters with the time step size. We will come back to this point later on.

Let us consider now which would be a finite difference time discretization of problem (17), with $\tilde{\boldsymbol{u}}$ solution of (11). To fix ideas, let us apply the generalized trapezoidal rule. Consider a uniform partition of $[0,T]$ of size δt, and for a time dependent function f let f^n denote an approximation to it at $t^n = n\delta t$, $\delta f^n := f^{n+1} - f^n$, $\delta_t f^n := \delta f^n/\delta t$ and $f^{n+\theta} = \theta f^{n+1} + (1-\theta) f^n$, with $1/2 \leqslant \theta \leqslant 1$. The generalized trapezoidal rule applied to (17) leads to the following fully discrete variational problem: given $\boldsymbol{u}_h^n$ and $\tilde{\boldsymbol{u}}^n$, find $\boldsymbol{u}_h^{n+1}$, p_h^{n+1} and $\tilde{\boldsymbol{u}}^{n+1}$ by solving

$$\begin{aligned}
&(\delta_t \boldsymbol{u}_h^n, \boldsymbol{v}_h) + \nu(\nabla \boldsymbol{u}_h^{n+\theta}, \nabla \boldsymbol{v}_h) + \langle \boldsymbol{u}_h^{n+\theta} \cdot \nabla \boldsymbol{u}_h^{n+\theta}, \boldsymbol{v}_h \rangle \\
&\quad - (p_h^{n+1}, \nabla \cdot \boldsymbol{v}_h) + (q_h, \nabla \cdot \boldsymbol{u}_h^{n+\theta}) - \langle \boldsymbol{v}_h, \boldsymbol{f}^{n+\theta} \rangle \\
&\quad + (\delta_t \tilde{\boldsymbol{u}}^n, \boldsymbol{v}_h) + \langle \tilde{\boldsymbol{u}}^{n+\theta} \cdot \nabla \boldsymbol{u}_h^{n+\theta}, \boldsymbol{v}_h \rangle - \langle \tilde{\boldsymbol{u}}^{n+\theta}, \tilde{\boldsymbol{u}}^{n+\theta} \cdot \nabla \boldsymbol{v}_h \rangle \\
&\quad - \sum_K \langle \tilde{\boldsymbol{u}}^{n+\theta}, \nu \Delta \boldsymbol{v}_h + \boldsymbol{u}_h^{n+\theta} \cdot \nabla \boldsymbol{v}_h + \nabla q_h \rangle_K = 0, \qquad (22)
\end{aligned}$$

$$\delta_t \tilde{\boldsymbol{u}}^n + \frac{1}{\tau^{n+\theta}} \tilde{\boldsymbol{u}}^{n+\theta} = \boldsymbol{r}_{u,h}^{n+\theta}, \qquad (23)$$

for all $[\boldsymbol{v}_h, q_h] \in \mathcal{V}_{0,h}^d \times \mathcal{Q}_{0,h}$ (we have assumed $\boldsymbol{f}$ continuous in time, otherwise $\boldsymbol{f}^{n+\theta}$ has to be understood as a time average between t^n and t^{n+1}). In (23) it is understood that the time derivative in $\boldsymbol{r}_{u,h}^{n+\theta}$ is already discretized. From this equation we can obtain $\tilde{\boldsymbol{u}}^{n+\theta}$ and insert it into (22). Obviously, the result will depend on $\tilde{\boldsymbol{u}}^n$, and thus the subscales *need to be tracked in time*.

Eq. (23) can be considered the "natural" choice for the time integration of the equation for the subscales, in the sense that they are integrated using the same scheme as the finite element component of the velocity. Likewise, if we had first discretized the continuous Navier–Stokes equations in time and then applied the splitting $\boldsymbol{u}^n = \boldsymbol{u}_h^n + \tilde{\boldsymbol{u}}^n$ we would have arrived also to (22), (23) (with the adequate modeling of the subscales). However, there is also the possibility of using a different time integration for $\boldsymbol{u}_h$ and $\tilde{\boldsymbol{u}}$. For example, assuming given a guess for $\tilde{\boldsymbol{u}}^{n+1}$ to evaluate τ^{n+1} and $\boldsymbol{r}_{u,h}^{n+1}$, within the time interval $[t^n, t^{n+1}]$ we could consider the *time continuous* equation for $\tilde{\boldsymbol{u}}$

$$\partial_t \tilde{\boldsymbol{u}} + \frac{1}{\tau^{n+\alpha}} \tilde{\boldsymbol{u}} = \boldsymbol{r}_{u,h}^{n+\alpha},$$

with $0 \leqslant \alpha \leqslant 1$, which can be integrated to yield

$$\tilde{\boldsymbol{u}}^{n+1} = (\tilde{\boldsymbol{u}}^n - \tau^{n+\alpha} \boldsymbol{r}_{u,h}^{n+\alpha}) \exp\left(-\frac{\delta t}{\tau^{n+\alpha}}\right) + \tau^{n+\alpha} \boldsymbol{r}_{u,h}^{n+\alpha}. \qquad (24)$$

Remember that both $\tau^{n+\alpha}$ and $\boldsymbol{r}_{u,h}^{n+\alpha}$ depend on $\tilde{\boldsymbol{u}}^{n+1}$, and therefore (24) is a nonlinear algebraic equation for this subscale (except if $\alpha = 0$, of course), which can be solved for example using the strategy proposed in [7], or simply linearized and solved iteratively.

Remark 8. Even though we are considering $\frac{1}{2} \leqslant \theta \leqslant 1$, (23) makes sense also for $\theta = 0$ (explicit integration of the subscales), case in which it yields $\tilde{\boldsymbol{u}}^{n+1} = (1 - \delta t/\tau^n)\tilde{\boldsymbol{u}}^n + \delta t \boldsymbol{r}_{u,h}^n$. This expression corresponds also to (24) with $\alpha = 0$ and expanding the exponential to first order in $\delta t/\tau^n$.

3.2. Why the stabilization parameter must depend on δt (but this is not enough)

Let us consider Eq. (23) and re-write it as

$$\tilde{\boldsymbol{u}}^{n+\theta} = \left(\frac{1}{\theta \delta t} + \frac{1}{\tau^{n+\theta}}\right)^{-1} \left(\boldsymbol{r}_{u,h}^{n+\theta} + \frac{1}{\theta \delta t} \tilde{\boldsymbol{u}}^n\right). \qquad (25)$$

From this expression we see that the residual of the momentum equation is multiplied by

$$\tau_t := \left(\frac{1}{\theta \delta t} + \frac{1}{\tau^{n+\theta}}\right)^{-1}. \qquad (26)$$

This is what can be considered the stabilization parameter for the transient incompressible Navier–Stokes equations. Expressions with asymptotic behavior similar to (26) in terms of h, ν, $|\boldsymbol{u}_h|$ and δt can be often found in the literature (see, e.g., [36,38]). The way to motivate it can be explained in a simplified way by saying that the temporal derivative of the velocity is considered as a reaction-like term (with a zero order derivative) with factor $1/(\theta \delta t)$, after considering for a given time step the equations discretized in time. This explanation can be found for example in [16], or in [30], where it motivates a careful design of the stabilization parameters for reaction dominated problems.

In [2] there is a study of the *instability* encountered when the ASGS method is used and (25) is replaced by the simplified equation

$$\tilde{\boldsymbol{u}}^{n+\theta} = \tau^{n+\theta} \boldsymbol{r}_{u,h}^{n+\theta}, \qquad (27)$$

that corresponds to what we have called quasi-static subscales. It is shown in the reference mentioned that for the Stokes time continuous problem the Schur complement matrix for the pressure is not uniformly invertible, and this property is inherited as $\delta t \to 0$ if h, and therefore $\tau^{n+\theta}$, remains fixed (the case $\theta = 1$ is considered in [2]).

It is easily shown that the instability described disappears if

$$\delta t \geqslant C \tau^{n+\theta}, \qquad (28)$$

where C is a positive constant. This is a condition that appears very often and about which there are several remarks to be made:

- As it has been mentioned, under condition (28) the instability problems described in [2] for the ASGS method do not appear. This condition prevents the possibility of letting $\delta t \to 0$ while keeping h fixed.
- In fact, if (28) holds it is irrelevant from the analysis point of view if the residual in (25) is multiplied by τ_t defined in (26) or simply by $\tau^{n+\theta}$, since this parameter and τ_t have the same asymptotic behavior in terms of h, ν and $|\boldsymbol{u}_h|$.
- Condition (28) was needed in the analysis of the stabilization with orthogonal subscales for the convection–diffusion equation analyzed in [14], also considering time dependent subscales. This point is further elaborated in Section 4.

From this discussion it seems clear that the stabilization parameter and the time step size *must be related in classical stabilized finite element methods*. This is clear from the heuristic arguments presented in the references mentioned above, the instability described in [2] for the ASGS method and the reasons found to comply with condition (28) just mentioned. However, we have not mentioned yet the fact that *in (25) we are tracking the subscales in time*. This has two major benefits, which justifies why taking the stabilization parameter as indicated by (26) *is not enough:*

- If, as it is done in [16,36,38], among other references, the stabilization parameter adopted has an expression similar to (26) but the subscales are not considered time dependent, *the steady-state solution depends on the time step size*. This is clearly not an optimal situation. The amount of stabilization will depend on the way the equations are integrated to the steady-state. This does not happen if expression (25) is used. It can be easily checked that, when the steady-state is reached, (27) (now without any superscript) is recovered.
- We will obtain stability *for all* δt *and* h*, without any need to satisfy (28)*. This is particularly relevant, since it allows us to use *arbitrary combinations of* h *and* δt. In other words, we may use what could be called *anisotropic* space–time discretizations. This stability analysis for the linearized problem is presented in Section 4. Of course it is possible to use directly (26) without considering time dependent subscales, and in that case (28) is automatically verified. However, that would lead to stability estimates that become meaningless *in space* when $\delta t \to 0$.

3.3. Tracking of subscales along the nonlinear process

Up to now we have considered the effect of the term $(\partial_t \tilde{\boldsymbol{u}}, \boldsymbol{v}_h)$ in (20) and of $\partial_t \tilde{\boldsymbol{u}}$ in (11). In this subsection we describe the effect of the other two terms in (20). Summarizing, $\langle \tilde{\boldsymbol{u}} \cdot \nabla \boldsymbol{u}_h, \boldsymbol{v}_h \rangle$ allows us to guarantee global conservation of momentum, whereas $-\langle \tilde{\boldsymbol{u}}, \tilde{\boldsymbol{u}} \cdot \nabla \boldsymbol{v}_h \rangle$ may be understood as the term coming from the subgrid-scale tensor in a LES approach.

3.3.1. Conservation of momentum

Let us start by analyzing the effect of $\langle \tilde{\boldsymbol{u}} \cdot \nabla \boldsymbol{u}_h, \boldsymbol{v}_h \rangle$. The purpose of what follows is to present a version of the results in [29], simplified and adapted to the present setting.

Let $\mathscr{V}_h^d$ be the velocity finite element space without imposing the Dirichlet boundary conditions, that is, with degrees of freedom also associated to the boundary nodes. Let $\boldsymbol{t}$ be the stress vector (traction) on the boundary Γ and consider the following augmented problem instead of (17):

$$
\begin{aligned}
&(\partial_t \boldsymbol{u}_h, \boldsymbol{v}_h) + \nu(\nabla \boldsymbol{u}_h, \nabla \boldsymbol{v}_h) + \langle \boldsymbol{u}_h \cdot \nabla \boldsymbol{u}_h, \boldsymbol{v}_h \rangle - (p_h, \nabla \cdot \boldsymbol{v}_h) \\
&\quad + (q_h, \nabla \cdot \boldsymbol{u}_h) - \langle \boldsymbol{v}_h, \boldsymbol{f} \rangle - \langle \boldsymbol{v}_h, \boldsymbol{t} \rangle_\Gamma + (\partial_t \tilde{\boldsymbol{u}}, \boldsymbol{v}_h) + \langle \tilde{\boldsymbol{u}} \cdot \nabla \boldsymbol{u}_h, \boldsymbol{v}_h \rangle \\
&\quad - \langle \tilde{\boldsymbol{u}}, \tilde{\boldsymbol{u}} \cdot \nabla \boldsymbol{v}_h \rangle - \sum_K \langle \tilde{\boldsymbol{u}}, \nu \Delta \boldsymbol{v}_h + \boldsymbol{u}_h \cdot \nabla \boldsymbol{v}_h + \nabla q_h \rangle_K = 0,
\end{aligned}
$$

where now $\boldsymbol{v}_h \in \mathscr{V}_h^d$ (not just $\mathscr{V}_{h,0}^d$). Considering $d = 3$ and taking for example $\boldsymbol{v}_h = (1,0,0)$ and $q_h = 0$, this equation yields

$$
\begin{aligned}
&\int_\Omega [\partial_t (u_{h,1} + \tilde{u}_1) - u_{h,1} \nabla \cdot \boldsymbol{u}_h] \, \mathrm{d}\Omega + \int_\Omega \tilde{\boldsymbol{u}} \cdot \nabla u_{h,1} \, \mathrm{d}\Omega \\
&\quad + \int_\Gamma u_{h,1} \boldsymbol{u}_n \cdot \boldsymbol{n} \, \mathrm{d}\Gamma = \int_\Omega f_1 \, \mathrm{d}\Omega + \int_\Gamma t_1 \, \mathrm{d}\Gamma,
\end{aligned}
$$

where now the zero Dirichlet condition for the velocity is not explicitly required. This statement provides *global* momentum conservation if

$$
-\int_\Omega u_{h,1} \nabla \cdot \boldsymbol{u}_h \, \mathrm{d}\Omega + \int_\Omega \tilde{\boldsymbol{u}} \cdot \nabla u_{h,1} \, \mathrm{d}\Omega = 0. \tag{29}
$$

This is implied by the continuity equation obtained by taking $\boldsymbol{v}_h = \boldsymbol{0}$

$$
(q_h, \nabla \cdot \boldsymbol{u}_h) - \sum_K \langle \tilde{\boldsymbol{u}}, \nabla q_h \rangle_K = 0, \tag{30}
$$

provided $\mathscr{V}_h / \mathbb{R} \subseteq \mathscr{Q}_{h,0}$, that is to say, the velocity component $u_{h,1}$ belongs to the pressure space ($u_{h,1}$ can be considered modulo constants, since they do not affect neither the first nor the second terms in (29)). This holds, in particular, for the "natural" choice $\mathscr{V}_h / \mathbb{R} = \mathscr{Q}_{h,0}$, that is to say, equal velocity–pressure interpolations. For the standard Galerkin method, *this condition is impossible to be satisfied*, since equal interpolation does not satisfy the inf–sup condition. As a conclusion, *the term* $\langle \tilde{\boldsymbol{u}} \cdot \nabla \boldsymbol{u}_h, \boldsymbol{v}_h \rangle$ *provides global momentum conservation*, since without it in the discrete momentum equation, we would have obtained $-\int_\Omega u_{h,1} \nabla \cdot \boldsymbol{u}_h \, \mathrm{d}\Omega = 0$ instead of (29), which is not implied by (30).

3.3.2. A door to turbulence

Let us conclude this section with some speculative comments on the contribution of the term $-\langle \tilde{\boldsymbol{u}}, \tilde{\boldsymbol{u}} \cdot \nabla \boldsymbol{v}_h \rangle$. In the

standard large eddy simulation (LES) approach to solve turbulent flows (see e.g., [34,35]) an equation is obtained for the large, filtered scales of the flow, which we will denote with an overbar. This equation includes an extra term when compared with the incompressible Navier–Stokes equations (1), (2): the divergence of the so-called *residual stress tensor* or *subgrid-scale tensor* $\boldsymbol{R} := \overline{\boldsymbol{u}\otimes\boldsymbol{u}} - \bar{\boldsymbol{u}}\otimes\bar{\boldsymbol{u}}$. Tensor $\boldsymbol{R}$ has to be modeled in terms of $\bar{\boldsymbol{u}}$ to obtain a self-contained equation, a problem known as the *closure problem*, and, once this is done, the resulting LES equation can be solved numerically.

The residual stress tensor, $\boldsymbol{R}$, is often decomposed into the so-called Reynolds, Cross and Leonard stresses to keep the Galilean invariance of the original Navier–Stokes equation in the LES equation. This invariance is automatically inherited by the formulation presented in this paper and we observe that analogous terms to the various stress types are recovered in a "natural" way from our pure numerical approach (this was also the case in [27]). Let us have a look at this point. We first consider the last four terms in the material derivative (21) as they appear in the variational equation (17). The term $-\langle\tilde{\boldsymbol{u}},\tilde{\boldsymbol{u}}\cdot\nabla\boldsymbol{v}_h\rangle$ can be rewritten as

$$-\langle\tilde{\boldsymbol{u}},\tilde{\boldsymbol{u}}\cdot\nabla\boldsymbol{v}_h\rangle = -\langle\tilde{\boldsymbol{u}}\otimes\tilde{\boldsymbol{u}},\nabla\boldsymbol{v}_h\rangle \quad \text{(Reynolds stress)}, \tag{31}$$

while the addition of the other three terms becomes, after integration by parts,

$$\langle\boldsymbol{u}_h\cdot\nabla\boldsymbol{u}_h,\boldsymbol{v}_h\rangle - \langle\tilde{\boldsymbol{u}},\boldsymbol{u}_h\cdot\nabla\boldsymbol{v}_h\rangle + \langle\tilde{\boldsymbol{u}}\cdot\nabla\boldsymbol{u}_h,\boldsymbol{v}_h\rangle = -\langle\boldsymbol{u}_h\otimes\boldsymbol{u}_h,\nabla\boldsymbol{v}_h\rangle$$
$$\text{(Convection of the large scales)}, \tag{32}$$
$$-\langle\boldsymbol{u}_h\otimes\tilde{\boldsymbol{u}}+\tilde{\boldsymbol{u}}\otimes\boldsymbol{u}_h,\nabla\boldsymbol{v}_h\rangle \quad \text{(Cross stress)}. \tag{33}$$

If we now pay attention to the convective term of the residual in the subscale equation (11) and take, for simplicity, $\mathscr{P} = I$, we observe that

$$\langle(\boldsymbol{u}_h+\tilde{\boldsymbol{u}})\cdot\nabla\boldsymbol{u}_h,\tilde{\boldsymbol{v}}\rangle = -\langle\boldsymbol{u}_h\otimes\boldsymbol{u}_h,\nabla\tilde{\boldsymbol{v}}\rangle \quad \text{(Leonard stress)} \tag{34}$$
$$-\langle\boldsymbol{u}_h\otimes\tilde{\boldsymbol{u}},\nabla\tilde{\boldsymbol{v}}\rangle. \tag{35}$$

Hence, we can effectively conclude that the modifications introduced by the presence of the divergence of $\boldsymbol{R}$ in the LES equations are somehow automatically included in our subgrid-scale stabilized finite element approach. So far we have given an interpretation to (32)–(35) as contributions from the Galerkin, stabilization and conservation of momentum terms and also from the equation driving the dynamic evolution of the subscales (11). In the present formulation, the remaining Reynolds stress term, (31), is then considered to account for the *direct* subscale "turbulent effects" onto the large, resolvable, scales.

How good our formulation will work as a turbulent model will mainly depend on the validity of the approximation made to derive the evolution equation for the subscales (11), being the ASGS or the OSS methods two available possibilities. In order to check this performance, benchmark problems for turbulent flows should be used. A widely used benchmark problem is the decay of isotropic turbulence. Our model should be able to reproduce the Kolmogorov energy cascade in the wavenumber Fourier space that displays an inertial range, where $E(k,t) \sim C_K\varepsilon^{2/3}k^{-5/3}$ (ε being the energy dissipation rate, k the wavenumber modulus, C_K the Kolmogorov constant in energy space and E the kinetic energy). The model should be also able to capture the appropriate decay in time of energy, enstrophy and other related statistical variables. Other more intricate questions such as if the model allows for backscatter or if the dimension of the global attractor is properly reproduced could be also addressed. We remind that the heuristic estimate for this dimension is $\mathscr{N} \sim (L/\lambda_K)^3 \sim Re^{\frac{9}{4}}$ (where λ_K is the Kolmogorov length scale) and that the closest estimate analytically proved is (roughly) $(L/\lambda_K)^{4.8}$ (see [17]). Another standard test for turbulence is the turbulent channel flow. In this case the model should be able to approximate the turbulent boundary layer that, according to Prandtl theory, exhibits a log behavior after the laminar sublayer. Finally, we should mention that in an attempt to find a more mathematical foundation for the LES approach to turbulence, the concept of *suitable approximations* to the Navier–Stokes equations has been introduced in [20,21]. It is expected that approximate solutions converge (in a weak sense) to *suitable solutions*. This seems to be the case for low order finite elements and the *standard Galerkin method* [19]. Hopefully, our *enhanced formulations* will have this property.

The original idea of using the multiscale formulation with local approximation to the fine scales to compute turbulent flows was already pointed out in [11] and later reintroduced in [7,28], and further elaborated in [25]. Very good results were obtained for fully developed and transitional turbulent flows. In fact, some promising results of numerical simulation of turbulent flows *only* with stabilization can be found in [23,15].

Let us conclude noting that the term $-\langle\tilde{\boldsymbol{u}},\tilde{\boldsymbol{u}}\cdot\nabla\boldsymbol{v}_h\rangle$ has been identified with the *direct* contribution of the subscale turbulent effect onto the large scales. However, all terms involving the subscales are indirectly affected by the turbulence effects because the subscales are obtained from the nonlinear equation (11) that involves (34), (35). In fact, it is argued in [7] that $-\langle\tilde{\boldsymbol{u}},\tilde{\boldsymbol{u}}\cdot\nabla\boldsymbol{v}_h\rangle$ has a little influence in the results. Let us also mention that instead of using an expression of $\tilde{\boldsymbol{u}}$ in terms of the residual, turbulence modeling can be attempted by giving directly an expression of $\tilde{\boldsymbol{u}}\otimes\tilde{\boldsymbol{u}}$ in terms of $\boldsymbol{u}_h$ in the spirit of Smagorinsky's model (see [27] and also [18] for a review).

4. Stability analysis of the linear problem

In this section we present the numerical analysis of the formulation in a simple setting. First, we consider the linear Oseen problem, that is, taking as advection velocity a *constant* field $\boldsymbol{a}$. As time integration scheme, we will consider only the backward Euler method, so that $\theta = 1$ in (22). The space of subscales will be taken orthogonal to the finite element space, and thus $\mathscr{P} = \Pi_h^{\perp}$ in (15) (remember that Π_h is the projection onto the velocity finite element space

$\mathcal{V}^d_{h,0}$). Finally, we will assume that $\Pi_h^{\perp}\boldsymbol{f}=\boldsymbol{0}$ ($\boldsymbol{f}$ is therefore a finite element function) or it is negligible, and we will also neglect $\Delta\boldsymbol{v}_h$ in (21). These assumptions are not at all essential, but allow us to simplify the analysis. Note that the stabilization parameter

$$\tau=\left[c_1\frac{\nu}{h^2}+c_2\frac{|\boldsymbol{a}|}{h}\right]^{-1} \tag{36}$$

will be constant.

Under all these conditions, the problem to be solved is: given $\boldsymbol{u}_h^n$, find $\boldsymbol{u}_h^{n+1}$, $\tilde{\boldsymbol{u}}^{n+1}$ and p_h^{n+1} such that

$$\begin{aligned}&(\delta\boldsymbol{u}_h^n,\boldsymbol{v}_h)+\nu\delta t(\nabla\boldsymbol{u}_h^{n+1},\nabla\boldsymbol{v}_h)+\delta t(\boldsymbol{a}\cdot\nabla\boldsymbol{u}_h^{n+1},\boldsymbol{v}_h)\\&\quad-\delta t(p_h^{n+1},\nabla\cdot\boldsymbol{v}_h)+\delta t(q_h,\nabla\cdot\boldsymbol{u}_h^{n+1})-\delta t\langle\boldsymbol{f}^{n+1},\boldsymbol{v}_h\rangle\\&\quad-\delta t(\tilde{\boldsymbol{u}}^{n+1},\boldsymbol{a}\cdot\nabla\boldsymbol{v}_h+\nabla q_h)=0,\end{aligned} \tag{37}$$

$$\delta\tilde{\boldsymbol{u}}^n+\delta t\tau^{-1}\tilde{\boldsymbol{u}}^{n+1}=-\delta t\Pi_h^{\perp}\left(\boldsymbol{a}\cdot\nabla\boldsymbol{u}_h^{n+1}+\nabla p_h^{n+1}\right). \tag{38}$$

In spite of the simplifying assumptions introduced, the *stability* analysis presented below highlights the effect of tracking the subscales in time from the analytical point of view. Let us summarize the results to be obtained in this section:

- First of all, we will prove a classical stability result that involves *both* the finite element component of the velocity and the velocity subscale, but not the pressure (Theorem 1).
- Then we will translate the stability obtained for $\tilde{\boldsymbol{u}}^{n+1}$ in terms of $\boldsymbol{u}_h^{n+1}$ and p_h^{n+1}. We will do this in dual norms introduced below (Theorems 2 and 3).
- The previous results hold *for all h and* δt. Under condition (26), we will be able to improve the previous results and prove stability in the norm usually employed in stabilized finite elements (Theorem 4).

Let us introduce some additional notation. Given a sequence $F=\{f^n\}$, with index n ranging from $n=1$ to $n=N$, the number of time intervals of the partition in time, we say that $F\in\ell^p(X)$ if $\sum_{n=1}^N\delta t\|f^n\|_X^p\leqslant C<\infty$, and $F\in\ell^\infty(X)$ if $\max_{n=1,\ldots,N}\|f^n\|_X\leqslant C<\infty$. Here and in what follows, C denotes a generic positive constant.

Given two sequences of functions defined in Ω, $F=\{f^n\}$ and $G=\{g^n\}$, with f^0 and g^0 also given, we will make use of the following discrete version of the integration-by-parts formula:

$$\sum_{n=0}^{N-1}\langle\delta f^n,g^{n+1}\rangle=-\sum_{n=0}^{N-1}\langle f^n,\delta g^n\rangle+\langle f^N,g^N\rangle-\langle f^0,g^0\rangle. \tag{39}$$

Let us recall now the classical inverse estimate that holds for quasi-uniform finite element partitions as those we are using (see, e.g., [3]). Given a finite element function f_h, there exists a constant C_{inv} such that

$$\|\nabla f_h\|\leqslant\frac{C_{\mathrm{inv}}}{h}\|f_h\|. \tag{40}$$

Before stating the stability results, let us finally remark the assumptions we will need on the data. Obviously, we will consider that $\boldsymbol{u}^0\in\boldsymbol{L}^2(\Omega)$, and therefore $\|\boldsymbol{u}_h^0\|$ and $\|\tilde{\boldsymbol{u}}^0\|$ will be bounded uniformly in h (see Remark 7). Concerning the force term, the classical assumption $\boldsymbol{f}\in L^2(0,T;\boldsymbol{H}^{-1}(\Omega))$ leads to stability at the expense of allowing the stability constant to depend on $1/\nu$ (see, e.g., [37]). Since *our interest is to prove stability estimates independent of* ν *and* $\boldsymbol{a}$, we will need to strengthen the previous assumption to $\boldsymbol{f}\in L^2(0,T;\boldsymbol{L}^2(\Omega))$. In fact, $\boldsymbol{f}\in L^1(0,T;\boldsymbol{L}^2(\Omega))$ would also work, and would be needed if we would consider the long term behavior $T\to\infty$, which is not our purpose here. Some small changes to the following analysis need to be made in this case. In what follows, we consider T fixed (and bounded). For the time discrete problem, the counterpart of $\boldsymbol{f}\in L^2(0,T;\boldsymbol{L}^2(\Omega))$ is $\{\boldsymbol{f}^n\}\in\ell^2(\boldsymbol{L}^2(\Omega))$.

Theorem 1. *Let* $\boldsymbol{u}_h^{n+1}$ *and* p_h^{n+1} *be the solution of* (37) *and* $\tilde{\boldsymbol{u}}^{n+1}$ *the solution of* (38)*. The following stability bounds hold for all* $\delta t>0$:

$$\begin{aligned}&\max_{n=0,\ldots,N-1}\left\{\|\boldsymbol{u}_h^{n+1}\|^2+\|\tilde{\boldsymbol{u}}^{n+1}\|^2\right\}\\&\quad+\sum_{n=0}^{N-1}\delta t(\nu\|\nabla\boldsymbol{u}_h^{n+1}\|^2+\|\tau^{-1/2}\tilde{\boldsymbol{u}}^{n+1}\|^2)\\&\quad\leqslant C\left(\sum_{n=0}^{N-1}\delta t\|\boldsymbol{f}^{n+1}\|^2+\|\boldsymbol{u}^0\|^2\right).\end{aligned} \tag{41}$$

Therefore, if $\{\boldsymbol{f}^n\}\in\ell^2(\boldsymbol{L}^2(\Omega))$ *and* $\boldsymbol{u}^0\in\boldsymbol{L}^2(\Omega)$, *we have that*

$$\begin{aligned}&\{\boldsymbol{u}_h^n\}\in\ell^\infty(\boldsymbol{L}^2(\Omega)),\quad\{\tilde{\boldsymbol{u}}^n\}\in\ell^\infty(\boldsymbol{L}^2(\Omega)),\\&\nu^{1/2}\{\boldsymbol{u}_h^n\}\in\ell^2(\boldsymbol{H}^1(\Omega)),\quad\{\tau^{-1/2}\tilde{\boldsymbol{u}}^n\}\in\ell^2(\boldsymbol{L}^2(\Omega)).\end{aligned}$$

Proof. In order to obtain stability bounds for the finite element solution, we test (37) by $\boldsymbol{v}_h=\boldsymbol{u}_h^{n+1}$ and $q_h=p_h^{n+1}$. Since $\boldsymbol{a}$ is constant and $\boldsymbol{u}_h^{n+1}=\boldsymbol{0}$ on $\partial\Omega$, we have that $(\boldsymbol{a}\cdot\nabla\boldsymbol{u}_h^{n+1},\boldsymbol{u}_h^{n+1})=0$. On the other hand, $(\boldsymbol{f}^{n+1},\boldsymbol{u}_h^{n+1})\leqslant\frac{\alpha}{2}\|\boldsymbol{f}^{n+1}\|^2+\frac{1}{2\alpha}\|\boldsymbol{u}_h^{n+1}\|^2$ for all $\alpha>0$. Adding up the resulting inequalities from $n=0$ to an arbitrary time level M and using the discrete Gronwall Lemma (see, e.g., [22]) with $\alpha>1$, we get

$$\begin{aligned}&\frac{1}{2}\|\boldsymbol{u}_h^{M+1}\|^2+\frac{1}{2}\sum_{n=0}^{M}\|\delta\boldsymbol{u}_h^n\|^2+\sum_{n=0}^{M}\delta t\nu\|\nabla\boldsymbol{u}_h^{n+1}\|^2\\&\quad-\sum_{n=0}^{M}\delta t(\tilde{\boldsymbol{u}}^{n+1},\boldsymbol{a}\cdot\nabla\boldsymbol{u}_h^{n+1}+\nabla p_h^{n+1})\\&\quad\leqslant C\left(\sum_{n=0}^{M}\delta t\|\boldsymbol{f}^{n+1}\|^2+\|\Pi_h(\boldsymbol{u}^0)\|^2\right).\end{aligned}$$

Now we can multiply (38) by $\tilde{\boldsymbol{u}}^{n+1}$, integrate over the whole domain and add up the result from $n=0$ to $n=M$. Doing that we obtain:

$$\frac{1}{2}\|\tilde{\boldsymbol{u}}^{M+1}\|^2+\frac{1}{2}\sum_{n=0}^{M}\|\delta\tilde{\boldsymbol{u}}^n\|^2+\sum_{n=0}^{M}\delta t\|\tau^{-1/2}\tilde{\boldsymbol{u}}^{n+1}\|^2$$
$$=-\sum_{n=0}^{M}\delta t\big(\tilde{\boldsymbol{u}}^{n+1},\Pi_h^{\perp}\big(\boldsymbol{a}\cdot\nabla\boldsymbol{u}_h^{n+1}+\nabla p_h^{n+1}\big)\big)+\frac{1}{2}\|\tilde{\boldsymbol{u}}^0\|^2.$$

Adding this equation to the previous inequality and noting that for any $L^2(\Omega)$-vector function $\boldsymbol{v}$ we have $(\tilde{\boldsymbol{u}}^{n+1},\boldsymbol{v})=\big(\tilde{\boldsymbol{u}}^{n+1},\Pi_h^{\perp}(\boldsymbol{v})\big)$, we arrive to

$$\|\boldsymbol{u}_h^{M+1}\|^2+\|\tilde{\boldsymbol{u}}^{M+1}\|^2+\sum_{n=0}^{M}\|\delta\boldsymbol{u}_h^n\|^2+\sum_{n=0}^{M}\|\delta\tilde{\boldsymbol{u}}^n\|^2$$
$$+\sum_{n=0}^{M}\delta tv\|\nabla\boldsymbol{u}_h^{n+1}\|^2+\sum_{n=0}^{M}\delta t\|\tau^{-1/2}\tilde{\boldsymbol{u}}^{n+1}\|^2$$
$$\leqslant C\left(\sum_{n=0}^{M}\delta t\|\boldsymbol{f}^{n+1}\|^2+\|\Pi_h(\boldsymbol{u}^0)\|^2+\|\tilde{\boldsymbol{u}}^0\|^2\right),$$

from where the theorem follows. □

The result just proved gives stability for both $\{\boldsymbol{u}_h^n\}$ and $\{\tilde{\boldsymbol{u}}^n\}$. However, we are interested *only* in the stability of the finite element solution (see Remark 10 below) The question that naturally arises is therefore what does the stability for the subscale mean in terms of the finite element solution. As it happens in stabilized finite element methods for stationary problems or considering quasi-static subscales [10,11], we will see that we will gain stability on the term

$$\boldsymbol{m}^n:=\boldsymbol{a}\cdot\nabla\boldsymbol{u}_h^n+\nabla p_h^n,\quad n=1,2,\ldots,N. \tag{42}$$

This provides control both on the convective derivative of the velocity and on the pressure gradient (note that pressure does not appear in the estimates of Theorem 1).

The question is now in which norm we will be able to prove stability of the sequence defined by (42). We need to consider two cases. In the general situation, without imposing any condition on δt and τ, we will prove stability in a rather weak dual norm. However, if we assume a condition of the form (26), it is possible to improve this stability to the classical norm of stabilized finite element methods.

Given a sequence $F=\{f^n\}$, of scalar or of vector functions defined on Ω, we define the following norm:

$$\|F\|_X:=\left(\sum_{n=1}^{N}\delta t\|f^n\|^2\right)^{1/2}+\sum_{n=0}^{N-1}\delta t\|\tau^{1/2}\delta_t f^n\|$$
$$+\max_{n=1,\ldots,N}\{\tau^{1/2}\|f^n\|\}, \tag{43}$$

which endows the space of sequences $X=\{F=\{f^n\}|F\in\ell^2(L^2(\Omega)),\{\tau^{1/2}\delta_t f^n\}\in\ell^1(L^2(\Omega)),\{\tau^{1/2}f^n\}\in\text{`}\ell^\infty(L^2(\Omega))\}$ of a Banach space structure. Note that $\{\delta_t f^n\}\in\ell^1(L^2(\Omega))$ and $F\in\ell^\infty(L^2(\Omega))$ certainly define strong topologies, but the factor $\tau^{1/2}$ prevents from any comparison between the different terms in (43).

Let now X' be the dual space of X, the duality pairing being

$$\langle F,G\rangle_{X\times X'}:=\sum_{n=1}^{N}\delta t\langle f^n,g^n\rangle,$$

with $F=\{f^n\}\in X$, $G=\{g^n\}\in X'$. The norm in X' is given by

$$\|G\|_{X'}=\sup_{F\in X,F\neq 0}\frac{\langle F,G\rangle_{X\times X'}}{\|F\|_X}. \tag{44}$$

Our main result is the following:

Theorem 2. *Assume that* $\{\boldsymbol{f}^n\}\in\ell^2(\boldsymbol{L}^2(\Omega))$ *and* $\boldsymbol{u}^0\in\boldsymbol{L}^2(\Omega)$. *Then, there is a constant* C *such that*

$$\|\{\tau^{1/2}\boldsymbol{m}^n\}\|_{X'}\leqslant C.$$

Proof. Let $\{\boldsymbol{v}^n\}\in X$ be an arbitrary sequence, and let us split $\boldsymbol{v}^n=\boldsymbol{v}_h^n+\tilde{\boldsymbol{v}}^n$, with $\boldsymbol{v}_h^n=\Pi_h(\boldsymbol{v}^n)$ and $\tilde{\boldsymbol{v}}^n=\boldsymbol{v}^n-\boldsymbol{v}_h^n$. We may write (38) as

$$\delta_t\tilde{\boldsymbol{u}}^n+\tau^{-1}\tilde{\boldsymbol{u}}^{n+1}=-\Pi_h^{\perp}(\boldsymbol{m}^{n+1}).$$

Multiplying this equation by $\tau^{1/2}\tilde{\boldsymbol{v}}^{n+1}$, integrating over Ω, adding up the result from $n=0$ to $N-1$, using formula (39) and finally using some simple inequalities, we find that

$$\sum_{n=0}^{N-1}\delta t\tau^{1/2}(\Pi_h^{\perp}(\boldsymbol{m}^{n+1}),\tilde{\boldsymbol{v}}^{n+1})$$
$$=-\sum_{n=0}^{N-1}\tau^{1/2}(\delta\tilde{\boldsymbol{u}}^n,\tilde{\boldsymbol{v}}^{n+1})-\sum_{n=0}^{N-1}\delta t\tau^{-1/2}(\tilde{\boldsymbol{u}}^{n+1},\tilde{\boldsymbol{v}}^{n+1})$$
$$=\sum_{n=0}^{N-1}\tau^{1/2}(\tilde{\boldsymbol{u}}^n,\delta\tilde{\boldsymbol{v}}^n)-\tau^{1/2}(\tilde{\boldsymbol{u}}^N,\tilde{\boldsymbol{v}}^N)+\tau^{1/2}(\tilde{\boldsymbol{u}}^0,\tilde{\boldsymbol{v}}^0)$$
$$-\sum_{n=0}^{N-1}\delta t\tau^{-1/2}(\tilde{\boldsymbol{u}}^{n+1},\tilde{\boldsymbol{v}}^{n+1})$$
$$\leqslant\max_{n=0,\ldots,N-1}\{\|\tilde{\boldsymbol{u}}^n\|\}\sum_{n=0}^{N-1}\delta t\tau^{1/2}\|\delta_t\tilde{\boldsymbol{v}}^n\|$$
$$+2\max_{n=0,\ldots,N}\{\|\tilde{\boldsymbol{u}}^n\|\}\tau^{1/2}\max_{n=0,\ldots,N}\{\|\tilde{\boldsymbol{v}}^n\|\}$$
$$+\left(\sum_{n=0}^{N-1}\delta t\|\tau^{-1/2}\tilde{\boldsymbol{u}}^{n+1}\|^2\right)^{1/2}\left(\sum_{n=0}^{N-1}\delta t\|\tilde{\boldsymbol{v}}^{n+1}\|^2\right)^{1/2}. \tag{45}$$

Theorem 1 allows us to conclude that

$$\langle\{\boldsymbol{v}^n\},\tau^{1/2}\{\Pi_h^{\perp}(\boldsymbol{m}^n)\}\rangle_{X\times X'}=\sum_{n=0}^{N-1}\delta t\tau^{1/2}(\Pi_h^{\perp}(\boldsymbol{m}^{n+1}),\tilde{\boldsymbol{v}}^{n+1})$$
$$\leqslant C\|\{\boldsymbol{v}^n\}\|_X. \tag{46}$$

The next step is to control the finite element component of $\{\boldsymbol{m}^n\}$. To this end, let us consider the momentum equation (37) with $q_h=0$ and $\boldsymbol{v}_h$ as defined before. Using arguments similar to those of the previous development, we have that

$$
\begin{aligned}
&\sum_{n=0}^{N-1}\delta t\tau^{1/2}(\Pi_h(\boldsymbol{m}^{n+1}),\boldsymbol{v}_h^{n+1})\\
&\quad=\sum_{n=0}^{N-1}\delta t\tau^{1/2}(\boldsymbol{a}\cdot\nabla\boldsymbol{u}_h^{n+1}+\nabla p_h^{n+1},\boldsymbol{v}_h^{n+1})\\
&\quad=\sum_{n=0}^{N-1}\delta t\tau^{1/2}\langle\boldsymbol{f}^{n+1},\boldsymbol{v}_h^{n+1}\rangle-\sum_{n=0}^{N-1}\tau^{1/2}(\delta\boldsymbol{u}_h^{n},\boldsymbol{v}_h^{n+1})\\
&\qquad-\sum_{n=0}^{N-1}\nu\delta t\tau^{1/2}(\nabla\boldsymbol{u}_h^{n+1},\nabla\boldsymbol{v}_h^{n+1})+\sum_{n=0}^{N-1}\delta t\tau^{1/2}(\tilde{\boldsymbol{u}}^{n+1},\boldsymbol{a}\cdot\nabla\boldsymbol{v}_h^{n+1})\\
&\quad\leqslant\tau^{1/2}\max_{n=1,\dots,N}\{\|\boldsymbol{v}_h^n\|\}\sum_{n=0}^{N-1}\delta t\|\boldsymbol{f}^{n+1}\|\\
&\qquad+\max_{n=0,\dots,N}\{\|\boldsymbol{u}_h^n\|\}\sum_{n=0}^{N-1}\delta t\tau^{1/2}\|\delta_t\boldsymbol{v}_h^n\|\\
&\qquad+2\max_{n=0,\dots,N}\{\|\boldsymbol{u}_h^n\|\}\tau^{1/2}\max_{n=0,\dots,N}\{\|\boldsymbol{v}_h^n\|\}\\
&\qquad+C\sum_{n=0}^{N-1}\delta t\nu^{1/2}\|\nabla\boldsymbol{u}_h^{n+1}\|\|\boldsymbol{v}_h^{n+1}\|\\
&\qquad+C\sum_{n=0}^{N-1}\delta t\tau^{-1/2}\|\tilde{\boldsymbol{u}}^{n+1}\|\|\boldsymbol{v}_h^{n+1}\|,
\end{aligned}
\tag{47}
$$

where for the last two terms we have used the inverse estimate (40) together with the definition (36) of τ, which in particular implies

$$
\frac{\nu}{h}\tau^{1/2}\leqslant C\nu^{1/2},\quad \frac{|\boldsymbol{a}|}{h}\tau^{1/2}\leqslant C\tau^{-1/2}.
$$

Using now the assumptions on the data, Cauchy's inequality for the last two terms of (47) and Theorem 1, it follows that

$$
\begin{aligned}
\langle\{\boldsymbol{v}^n\},\tau^{1/2}\{\Pi_h(\boldsymbol{m}^n)\}\rangle_{X\times X'}&=\sum_{n=0}^{N-1}\delta t\tau^{1/2}(\Pi_h(\boldsymbol{m}^{n+1}),\boldsymbol{v}_h^{n+1})\\
&\leqslant C\|\{\boldsymbol{v}^n\}\|_X.
\end{aligned}
\tag{48}
$$

The theorem follows from (46) and (48). □

Remark 9. Instead of considering $\mathscr{P}=\Pi_h^{\perp}$ in (15), with Π_h the projection onto the velocity finite element space $\mathscr{V}_{h,0}^d$, we could also have considered $\mathscr{P}=\Pi_h^{*,\perp}$, with Π_h^* the projection onto $\mathscr{V}_h^d$ (that is, the velocity space without boundary conditions). The previous proof could be easily adapted to obtain stability for $\|\tau^{1/2}\{\Pi_h(\boldsymbol{m}^n)\}\|_{X'}$ and $\|\tau^{1/2}\{\Pi_h^{*,\perp}(\boldsymbol{m}^n)\}\|_{X'}$. The remaining component of $\tau^{1/2}\{\boldsymbol{m}^n\}$ can be bounded using a mild inf–sup condition, as explained in [12], which holds in the case of equal velocity–pressure interpolation (see [12] for details).

In the particular case of the backward Euler time integration that we are considering in this Section, we can make use of the fact that

$$
\sum_{n=0}^{N-1}\|\delta\boldsymbol{u}_h^n\|^2+\sum_{n=0}^{N-1}\|\delta\tilde{\boldsymbol{u}}^n\|^2\leqslant C,
\tag{49}
$$

which is in fact a by-product of the proof of Theorem 1 (unfortunately, this property is not to be expected in other schemes such as the Crank–Nicolson time integration). In turn, the proof of Theorem 2 with slight modifications is applicable if the norm $\|\cdot\|_X$ defined in (43) is replaced by

$$
\|F\|_Y:=\left(\sum_{n=1}^{N}\max\{\delta t,\tau\}\|f^n\|^2\right)^{1/2}.
\tag{50}
$$

In fact, we have:

Theorem 3. *Assume that* $\{\boldsymbol{f}^n\}\in\ell^2(\boldsymbol{L}^2(\Omega))$ *and* $\boldsymbol{u}^0\in\boldsymbol{L}^2(\Omega)$. *Then, there is a constant* C *such that*

$$
\|\{\tau^{1/2}\boldsymbol{m}^n\}\|_{Y'}\leqslant C.
$$

Proof. The only terms that need to be bounded in a different way with respect to the proof of Theorem 2 are of the form

$$
\sum_{n=0}^{N-1}\tau^{1/2}(\delta\boldsymbol{u}^n,\boldsymbol{v}^{n+1})\leqslant\left(\sum_{n=0}^{N-1}\|\delta\boldsymbol{u}^n\|^2\right)^{1/2}\left(\sum_{n=1}^{N}\tau\|\boldsymbol{v}^n\|^2\right)^{1/2},
\tag{51}
$$

where $\boldsymbol{u}$ and $\boldsymbol{v}$ belong to the space of subscales in the bound analogous to (45) and belong to the finite element space in the bound analogous to (47). Due to the boundedness property (49), (51) is bounded by $C\|\{\boldsymbol{v}^n\}\|_Y$. The proof concludes as that of Theorem 2. □

From Theorem 3 we easily obtain our last result, which is nothing but a refinement when condition (26) holds:

Theorem 4. *Suppose that the stabilization parameter defined in* (36) *satisfies* $\tau\leqslant C\delta t$ *as* $h\to 0$ *and* $\delta t\to 0$, *and assume also that* $\{\boldsymbol{f}^n\}\in\ell^2(\boldsymbol{L}^2(\Omega))$ *and* $\boldsymbol{u}^0\in\boldsymbol{L}^2(\Omega)$. *Then, there is a constant* C *such that*

$$
\sum_{n=1}^{N}\delta t\|\tau^{1/2}\boldsymbol{m}^n\|^2\leqslant C.
$$

Proof. If $\tau\leqslant C\delta t$ it is immediately checked from definition (50) that $Y=\ell^2(L^2(\Omega))$. This space is reflexive, that is, $Y=Y'$, and thus Theorem 3 implies directly Theorem 4. □

Remark 10. One could consider that the *numerical solution* of the problem is $\boldsymbol{u}_h+\tilde{\boldsymbol{u}}$, with $\tilde{\boldsymbol{u}}$ the approximated subscale. However, we do not see any reason why this solution has to behave better than $\boldsymbol{u}_h$ alone. Clearly, we cannot expect *neither* $\boldsymbol{u}_h$ *nor* $\boldsymbol{u}_h+\tilde{\boldsymbol{u}}$ to have a convergence behavior in h towards the continuous solution $\boldsymbol{u}$ better than the finite element interpolant. If this is so for $\boldsymbol{u}_h$, there is no reason to think that $\boldsymbol{u}_h+\tilde{\boldsymbol{u}}$ will be better. The main point of the formulation is that taking into account $\tilde{\boldsymbol{u}}$ the finite element solution $\boldsymbol{u}_h$ has better convergence properties than the finite element solution with $\tilde{\boldsymbol{u}}=\boldsymbol{0}$, in the sense that the constants in the stability and convergence estimates do not depend on the coefficients of the equation and, in particular, do not blow up as $\nu\to 0$.

5. Numerical examples

In this section we present three simple numerical examples that illustrate the performance of the method. The first is a convergence test that shows that for solutions with a smooth behavior in time both quasi-static and transient subscales lead to the same optimal convergence rate. In the second example we demonstrate the improvement obtained when the subscales are tracked in time in the example introduced in [2]. Finally, the last example is the classical flow over a cylinder, for which considering transient subscales leads to better results, both in terms of accuracy (with higher amplitudes and frequencies, that is, less numerical dissipation) and of stability, eliminating some pressure oscillations in time encountered when the subscales are considered quasi-static. In all the cases we have used the ASGS method, that is, $\mathscr{P} = I$ (identity) in (15), (16).

5.1. A convergence test

In this example, already presented in [9], we consider the time dependent Navier–Stokes equations in the unit square with homogeneous Dirichlet boundary conditions and taking the force $\boldsymbol{f}$ and boundary and initial values to have the exact solution defined by

$$\boldsymbol{u} = 100h(t)(f(x)f'(y), -f'(x)f(y)), \quad p = 100x^2,$$

where

$$h(t) = \cos(\pi t)\mathrm{e}^{-t}, \quad f(x) = x^2(1-x)^2.$$

Uniform meshes of 10×10, 20×20, 40×40 and 80×80 bilinear elements have been used to discretize the computational domain. The time interval of the analysis is $[0, 1]$ and the viscosity is 0.1.

The objective of this test is to check the convergence of the time approximation to the exact solution using the method proposed here. To this end we compare the results obtained using transient subscales (TRS) to those obtained using quasi-static subscales (QSS) (see Remark 2). We compute the error as the discrete approximation to the L^2 norm of the difference between the exact and the approximated solution at time $t = 1$ and we normalize it using the discrete approximation to the L^2 norm of the exact solution. Numerical experiments have been performed using a first and a second order temporal discretization (Crank–Nicolson scheme) and several time step sizes. In the case of the second order approximation we have also considered a first and second order time integration of Eq. (23). The convergence of the velocity approximation is shown in Fig. 1, from where it is seen that stabilized approximation converges to the exact solution at the expected rate either using the time dependent or the quasi-static subscales (see Remark 9). We also note that the integration of the subgrid-scale equation (23) using a first or a second order method has little influence on the results.

5.2. Stability in the small time step limit

The second example, presented in [2], shows the instability of the approximation to the Stokes problem when quasi-static subscales are considered (recall that we are using the ASGS method in all the examples). It consists again of an exact solution problem in which the time dependent Navier–Stokes equations are solved in the unit square with Dirichlet boundary conditions taking the force $\boldsymbol{f}$ and boundary and initial values to have the exact (steady-state) solution defined by

$$\boldsymbol{u} = (\sin(\pi x - 0.7)\sin(\pi y + 0.2), \cos(\pi x - 0.7)\cos(\pi y + 0.2)),$$
$$p = \sin(\pi x)\cos(\pi y) + (\cos(1) - 1)\sin(1).$$

Numerical examples presented in [2] show that spurious oscillations in the pressure are found when the time step is small enough and that this effect is more dramatic when the order of the polynomial approximation is increased. We have solved this problem using different meshes for time step sizes $\delta t^n = 10^{-n}$ using a first order time approximation.

Fig. 2 shows the convergence of the approximation using bilinear elements at the first time step, while Fig. 3 shows the same results corresponding to the second time step. The instability mentioned can be seen in Fig. 2, as for a given mesh size the error increases when the time step is decreased. As a first order approximation is being used and the solution of the problem is steady, the error should decrease linearly with the time step size. This is not the case in the first step, neither using the quasi-static subscales as shown in [2], nor using transient subscales. However, as shown in Fig. 3, when the transient subscales are considered the instability is eliminated at the second time step. This behavior leads to consider the practical problem of the initial conditions for the subgrid-scale (we have taken them to be zero), which has not been considered here. It has to be noted that, in any case, the instability observed disappears as time advances and, obviously, the stationary solution is equally approximated using quasi-static and transient subscales.

The situation is different when higher order elements are used. Fig. 4 shows the convergence of the approximation using biquadratic elements while Fig. 5 shows the convergence of the approximation using bicubic elements, both at the first time step. Similar results are found for the second time step. From Figs. 4 and 5 it is seen that when quasi-static subscales are considered the method could not converge as the mesh is refined for small time steps. This is even more dramatic than the result presented in [2], where only a fixed mesh of 10×10 elements was considered. In the case of transient subscales, although some dependence of the error on the time step size is still observed, convergence under mesh refinement is always achieved. This effect is seen in Fig. 6, where pressure contours for different mesh sizes obtained using quasi-static and transient subscales are compared.

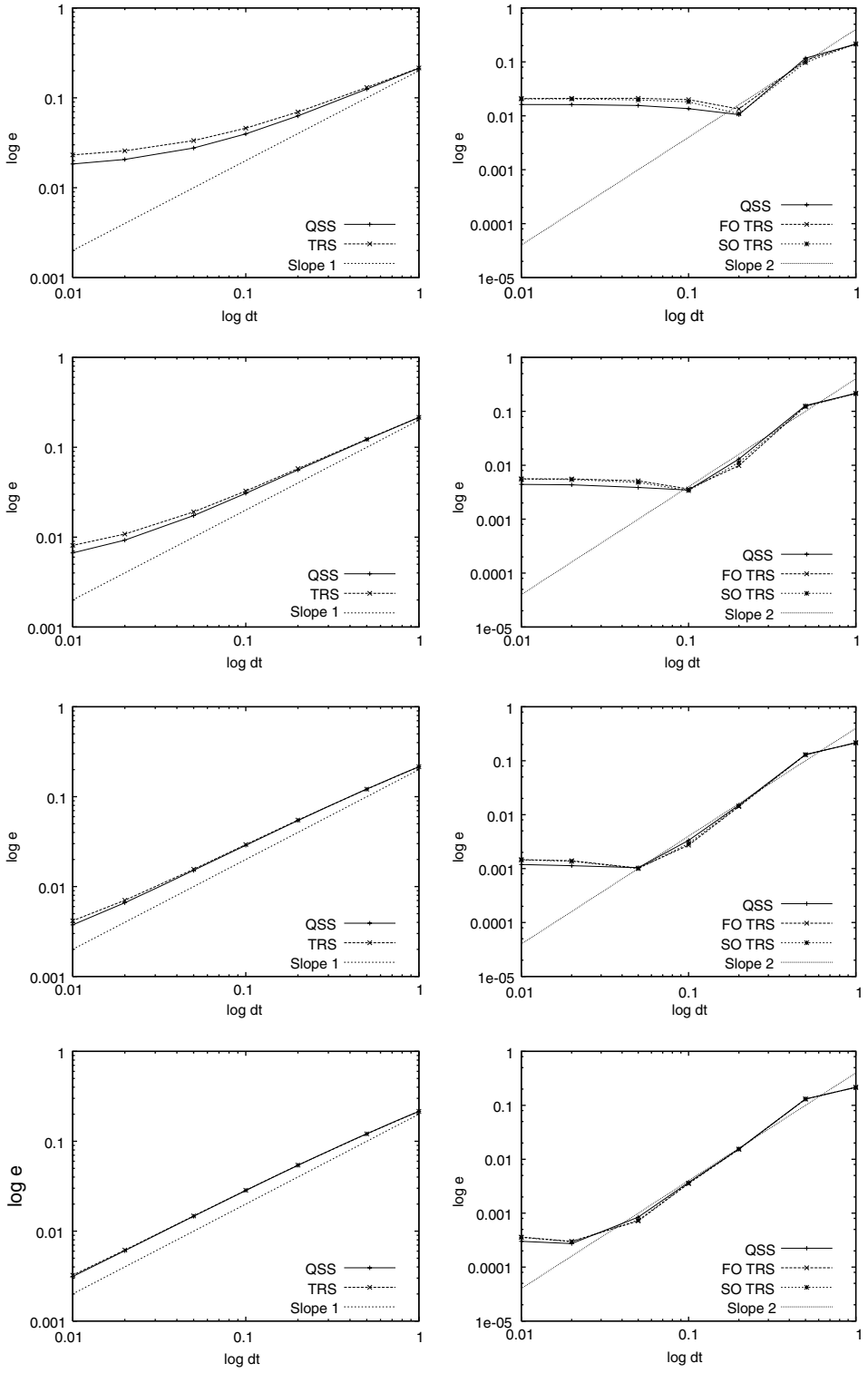

Fig. 1. Convergence of the time approximation using quasi-static subscales (QSS) and transient subscales (TRS). First order approximation on the left and second order approximation on the right. In the second order approximation first order (FO) or second order (SO) subscales are considered. From top to bottom meshes of sizes $h = 1/20$, $h = 1/40$ and $h = 1/80$. Note that the convergence curves loose the optimal slope in time (1 or 2) when the error becomes dominated by the spatial component.

5.3. Flow past a cylinder

The last example is the flow past a cylinder at $Re = 100$, a well known benchmark. The domain is $[0, 16] \times [0, 8] \setminus D$, where the cylinder D has a diameter 1 and is located at $(4, 4)$. A uniform velocity is prescribed at the inlet, zero y component is prescribed at $y = 0$ and $y = 8$ and zero traction is prescribed at the outlet. Two meshes have been used

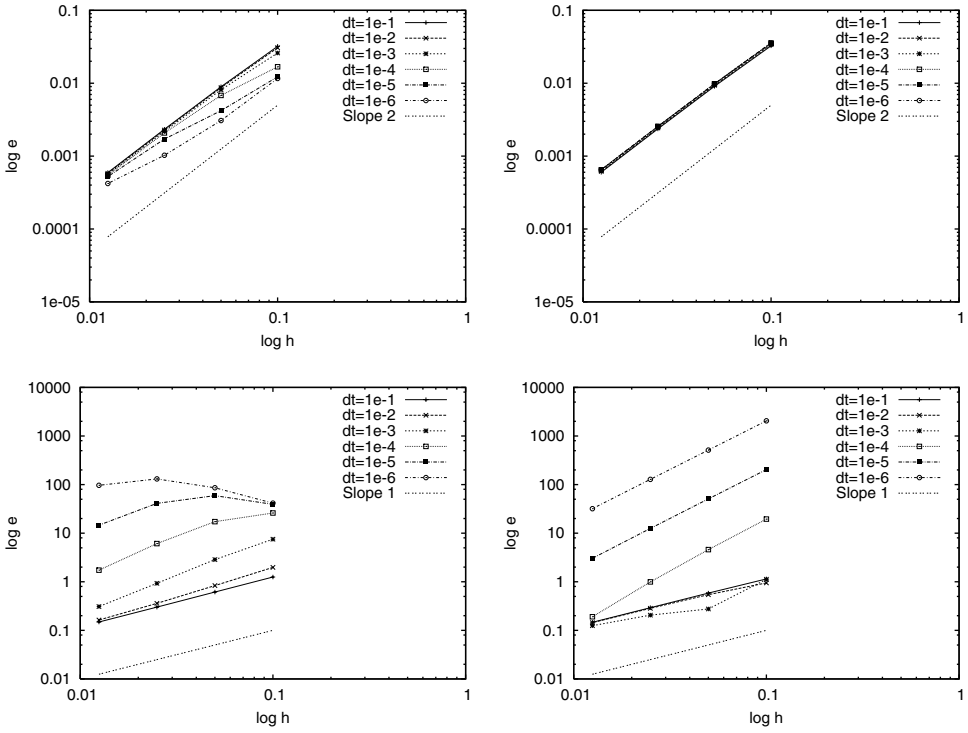

Fig. 2. Convergence of the approximation using bilinear elements at the first time step. Quasi-static subscales on the left and transient subscales on the right. Velocity error at the top and pressure error at the bottom.

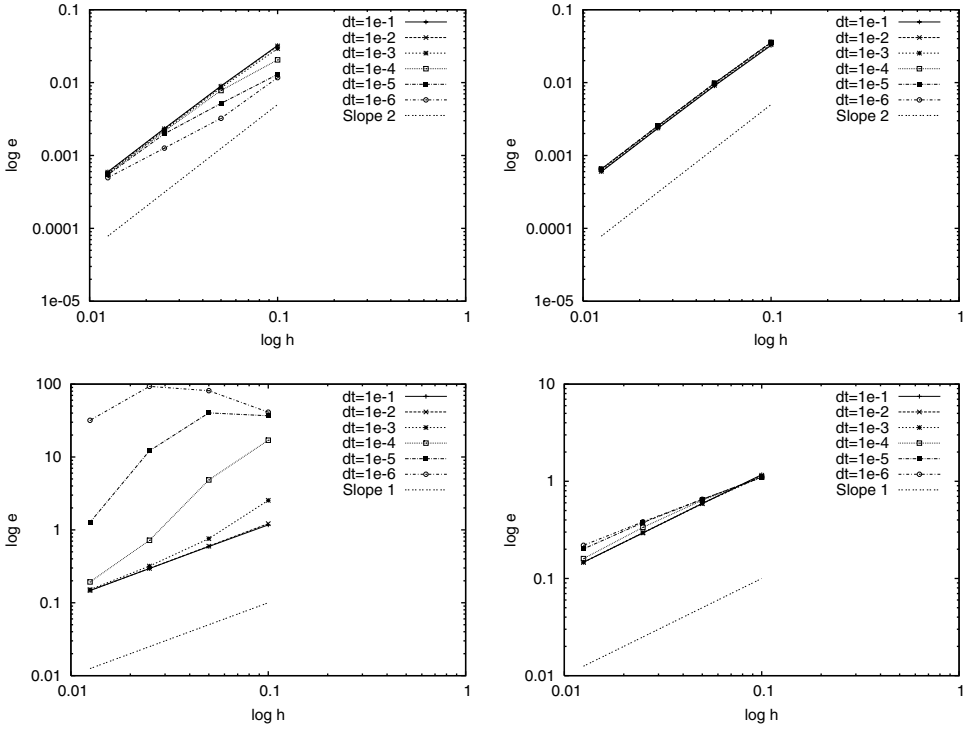

Fig. 3. Convergence of the approximation using bilinear elements at the second time step. Quasi-static subscales on the left and transient subscales on the right. Velocity error at the top and pressure error at the bottom.

to test the behavior of the method, a coarse one of 1360 nodes and a fine one of 5280. The results will be compared to those obtained using a reference mesh of 20,800 nodes.

The initial condition is $\boldsymbol{u} = (1, 0)$ except at the cylinder surface. From this initial condition the flow evolves to a symmetric solution that becomes unstable around $t = 100$

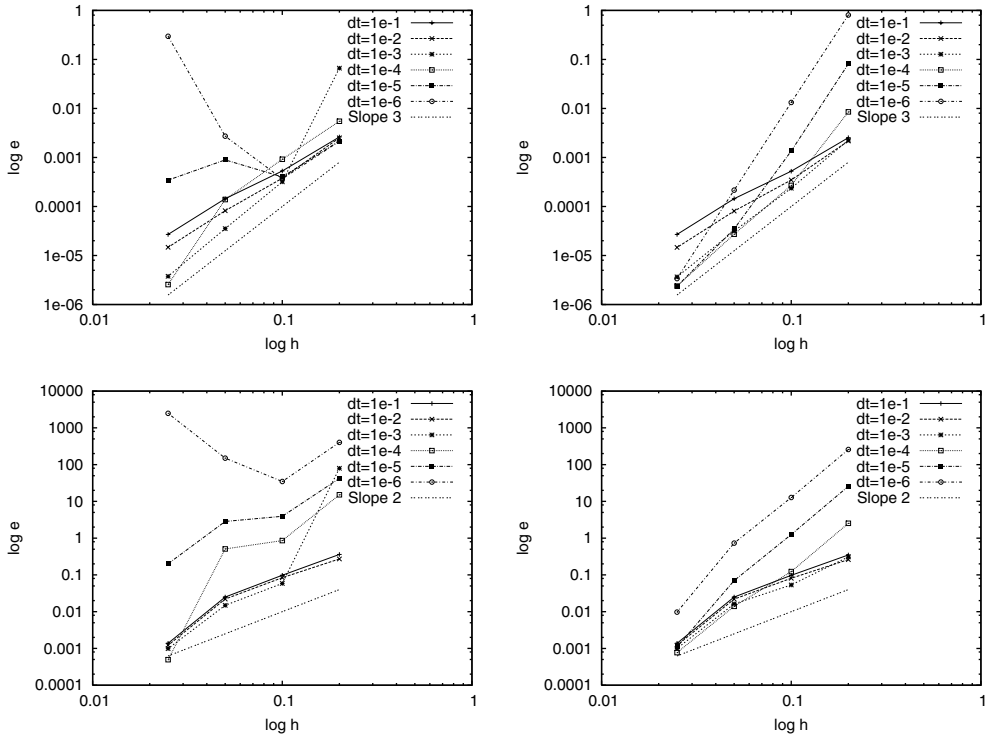

Fig. 4. Convergence of the approximation using biquadratic elements at the first time step. Quasi-static subscales on the left and transient subscales on the right. Velocity error at the top and pressure error at the bottom.

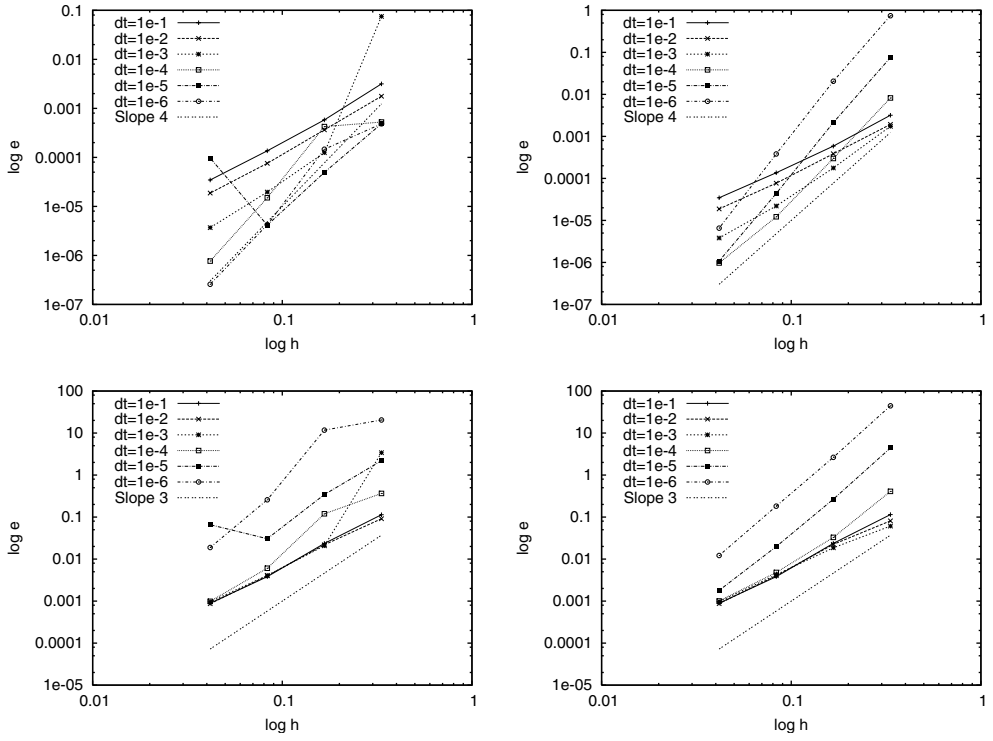

Fig. 5. Convergence of the approximation using bicubic elements at the first time step. Quasi-static subscales on the left and transient subscales on the right. Velocity error at the top and pressure error at the bottom.

and the characteristic vortex shedding appears. To visualize the problem setting, a pressure distribution snapshot in the fully developed regime is shown in Fig. 7. A second order method has been used with time step size $\delta t = 0.2$ and 10 Euler time steps have been performed at the beginning of the calculations for all the meshes. A convergence

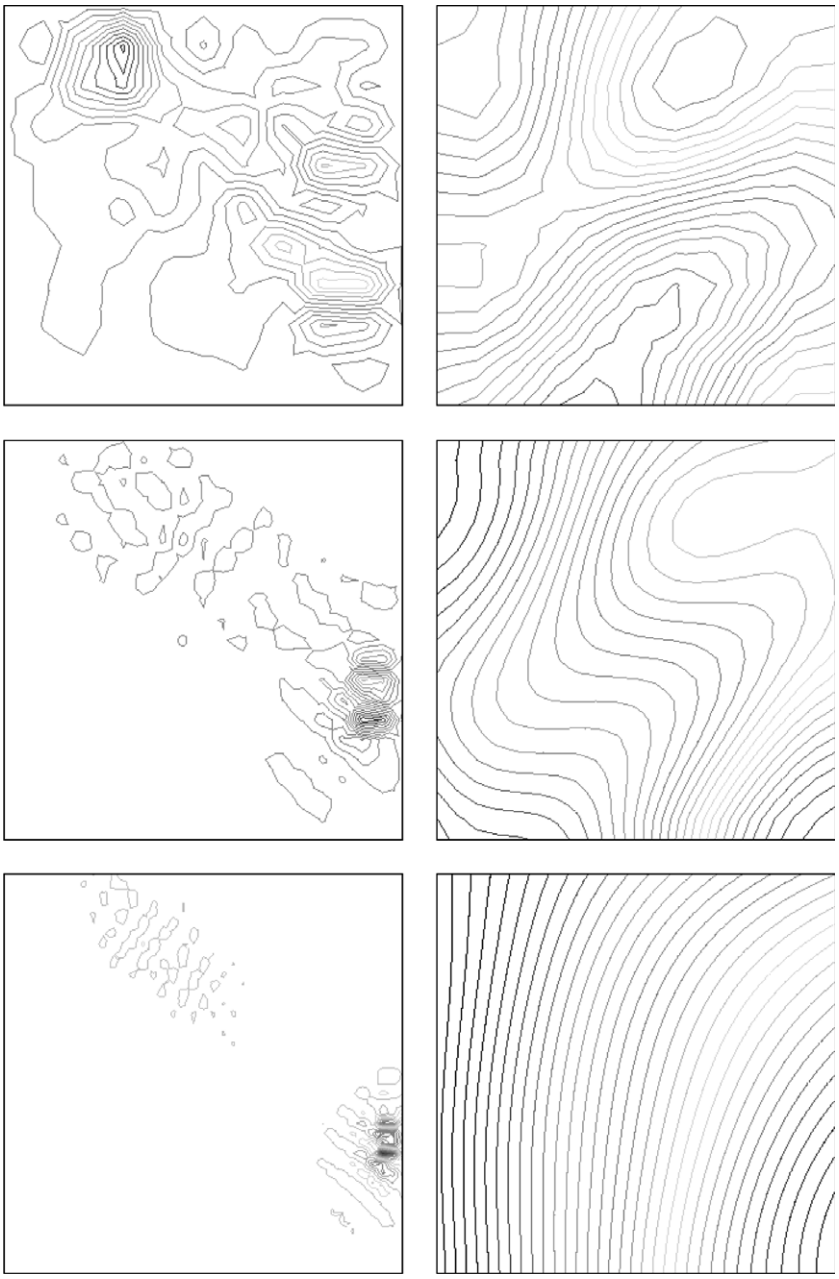

Fig. 6. Pressure contours for $\delta t = 10^{-6}$ and (from top to bottom) $h = 1/20$, $h = 1/40$ and $h = 1/80$ using biquadratic elements. Quasi-static subscales on the left and transient subscales on the right.

tolerance of 10^{-8} was required at each step, which was achieved typically after 8–10 Picard iterations.

Figs. 8 and 9 show the evolution of the x-velocity at point (6.15,4), Figs. 10 and 11 that of the y-velocity and Figs. 12 and 13 that of the pressure, always at the same point and for the two meshes considered, comparing the results obtained using quasi-static subscales and transient subscales to those obtained using the reference mesh. It can be seen from Figs. 8 and 9 how the use of the transient subscales gives a better mean value of the x-velocity when the flow is fully developed, specially in the coarse mesh. From Figs. 10 and 11 it can be observed how the use of the transient subscales gives a higher amplitude and a

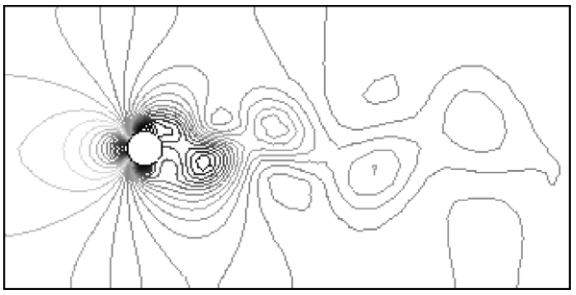

Fig. 7. Pressure distribution at $t = 160$.

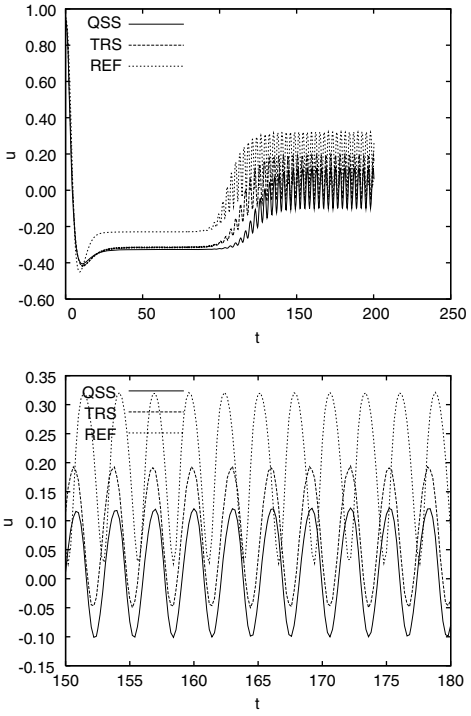

Fig. 8. Horizontal velocity evolution at (6.15,4.0) using the coarse mesh (top) and its detail (bottom).

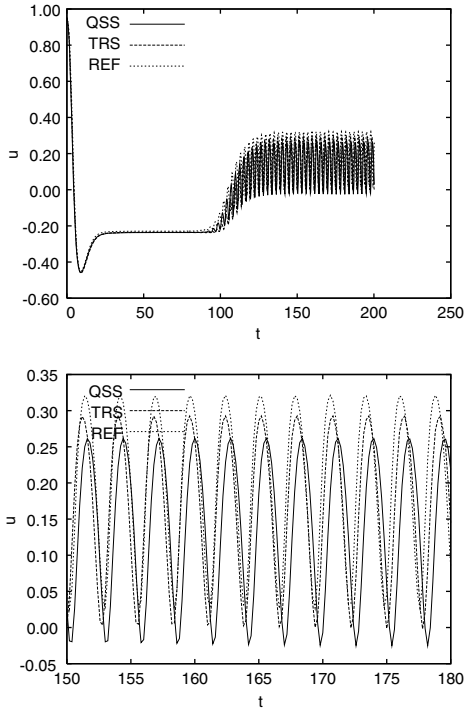

Fig. 9. Horizontal velocity evolution at (6.15,4.0) using the fine mesh (top) and its detail (bottom).

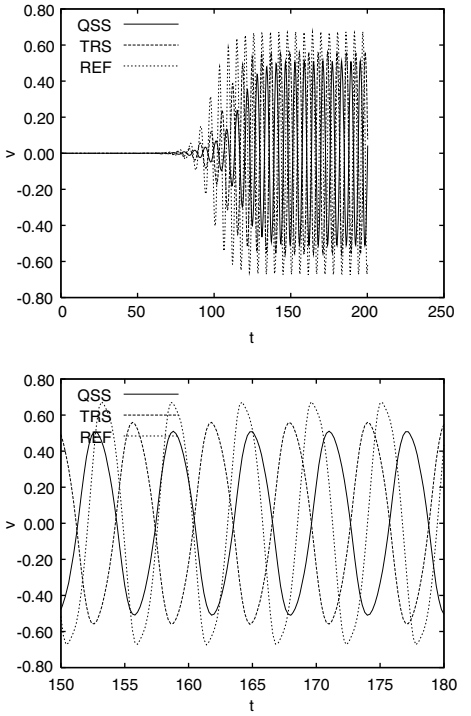

Fig. 10. Vertical velocity evolution at (6.15,4.0) using the coarse mesh (top) and its detail (bottom).

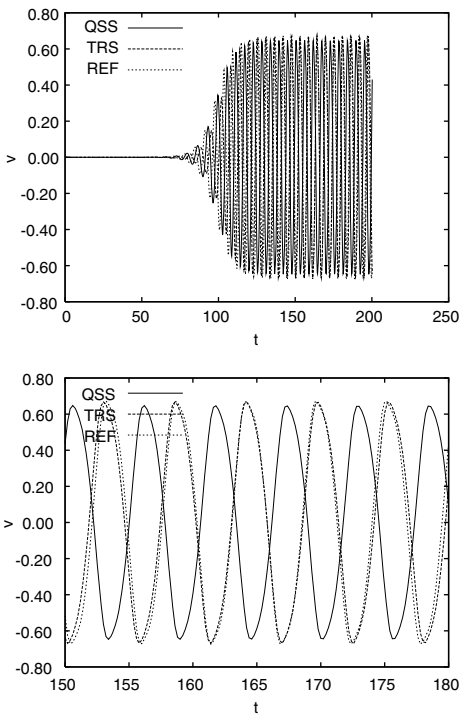

Fig. 11. Vertical velocity evolution at (6.15,4.0) using the fine mesh (top) and its detail (bottom).

higher frequency of the oscillation, that is to say, less numerical dissipation. Finally, in Fig. 12 some time step-to-time step oscillations can be observed when the quasi-static subscales are used and how these oscillations do not appear when transient subscales are considered. These oscillations, already reported in [11], depend on the length used in the definition of the stabilization parameters. They appear when there is a variation of the element size from

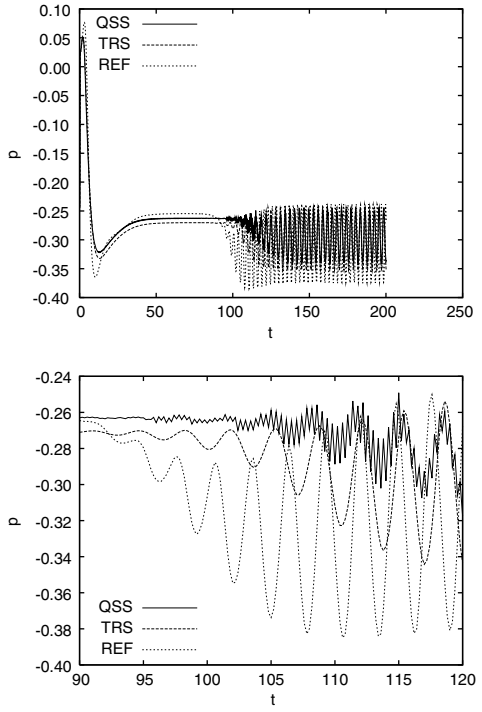

Fig. 12. Pressure evolution at (6.15,4.0) using the coarse mesh (top) and its detail (bottom).

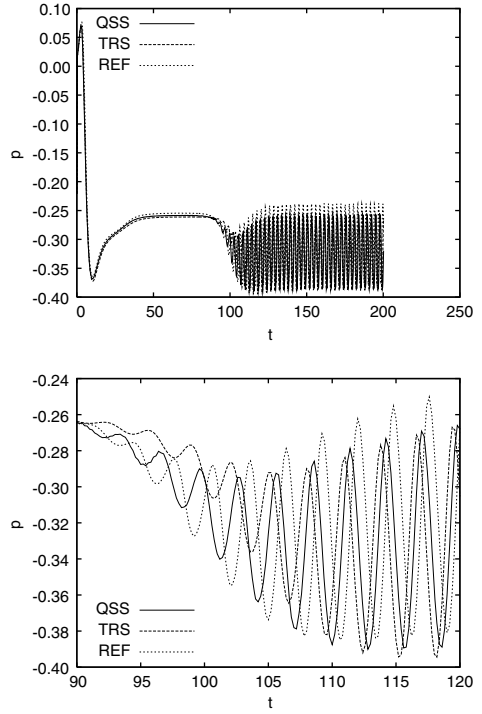

Fig. 13. Pressure evolution at (6.15,4.0) using the fine mesh (top) and its detail (bottom).

one element to another and they disappear if a fixed mesh size is used to define the stabilization parameter. From Fig. 13 it is seen that they also disappear in the fine mesh. In this case there is almost no gain in the pressure using transient subscales (but there is in the velocity, as shown in Figs. 9 and 11).

6. Conclusions

The main conclusion of this paper is simple: we believe it is worth to track the subscales in time in a variational multiscale approach to the transient incompressible Navier–Stokes equations and to take into account all their contributions in the convective term.

The first and very simple reason is that it leads to global momentum conservation, a rare property. A second reason can be the door opened to turbulence modeling, although we have touched this point only marginally. What has been the main focus of this paper is the study of the advantages of tracking the subscales from the point of view of the time integration scheme. First, we have remarked that the resulting formulation leads in a natural way to the correct behavior of the stabilization parameters with the time step while steady-state solutions do not depend on it. Moreover, the conflict about the design of the stabilization terms for time dependent problems (either at the semi-discrete or the fully discrete level) disappears, since space and time discretization can be commuted. The numerical analysis shows that the method is stable (a simple setting has been analyzed here) and the numerical experiments show that the gain with respect to quasi-static subscales is notorious.

Acknowledgements

J. Principe and S. Badia would like to acknowledge the support received from the *Departament d'Universitats, Recerca i Societat de la Informació* of the *Generalitat de Catalunya* (Catalan Government) and the *European Social Fund* through a doctoral grant.

References

[1] C. Baiocchi, F. Brezzi, L.P. Franca, Virtual bubbles and Galerkin/least-squares type methods (Ga.L.S), Comput. Methods Appl. Mech. Engrg. 105 (1993) 125–141.
[2] P.B. Bochev, M.D. Gunzburger, R.B. Lehoucq, On stabilized finite element methods for the Stokes problem in the small time-step limit, Int. J. Numer. Methods Fluids 53 (2007) 573–597.
[3] S.C. Brenner, L.R. Scott, The Mathematical Theory of Finite Element Methods, Springer-Verlag, 1994.
[4] F. Brezzi, L.P. Franca, T.J.R. Hughes, A. Russo, $b = \int g$, Comput. Methods Appl. Mech. Engrg. 145 (1997) 329–339.
[5] A.N. Brooks, T.J.R. Hughes, Streamline upwind/Petrov–Galerkin formulations for convection dominated flows with particular emphasis on the incompressible Navier–Stokes equation, Comput. Methods Appl. Mech. Engrg. 32 (1982) 199–259.
[6] E. Burman, M.A. Fernández, A finite element method with edge oriented stabilization for the time-dependent Navier–Stokes equations: space discretization and convergence, under review.
[7] V.M. Calo, Residual based multiscale turbulence modeling: finite volume simulations of bypass transition, Ph.D. thesis, Department of Civil and Environmental Engineering, Stanford University, 2004.

[8] R. Codina, Stabilization of incompressibility and convection through orthogonal sub-scales in finite element methods, Comput. Methods Appl. Mech. Engrg. 190 (2000) 1579–1599.
[9] R. Codina, Pressure stability in fractional step finite element methods for incompressible flows, J. Comput. Phys. 170 (2001) 112–140.
[10] R. Codina, A stabilized finite element method for generalized stationary incompressible flows, Comput. Methods Appl. Mech. Engrg. 190 (2001) 2681–2706.
[11] R. Codina, Stabilized finite element approximation of transient incompressible flows using orthogonal subscales, Comput. Methods Appl. Mech. Engrg. 191 (2002) 4295–4321.
[12] R. Codina, J. Blasco, A finite element formulation for the Stokes problem allowing equal velocity–pressure interpolation, Comput. Methods Appl. Mech. Engrg. 143 (1997) 373–391.
[13] R. Codina, J. Blasco, Analysis of a pressure-stabilized finite element approximation of the stationary Navier–Stokes equations, Numer. Math. 87 (2000) 59–81.
[14] R. Codina, J. Blasco, Analysis of a stabilized finite element approximation of the transient convection–diffusion–reaction equation using orthogonal subscales, Comput. Visualiz. Sci. 4 (2002) 167–174.
[15] P.A.B. de Sampaio, P.H. Hallak, A.L.G.A. Coutinho, M.S. Pfeil, A stabilized finite element procedure for turbulent fluid–structure interaction using adaptive time–space refinement, Int. J. Numer. Methods Fluids 44 (2004) 673–693.
[16] T. Gelhard, G. Lube, M.A. Olshanskii, J.A. Starcke, Stabilized finite element schemes with LBB-stable elements for incompressible flows, J. Comput. Appl. Math. 177 (2005) 243–267.
[17] J. Gibbon, E. Titi, Attractor dimension and small length scale estimates for the three dimensional Navier–Stokes equations, Nonlinearity 10 (1997) 109–119.
[18] V. Gravemeier, The variational mulstiscale method for laminar and turbulent flow, Arch. Comput. Mech. – State of the Art Rev. 13 (2006) 249–324.
[19] J.L. Guermond, Finite-element-based Faedo–Galerkin weak solutions to the Navier–Stokes equations in the three-dimensional torus are suitable, J. Math. Pures Appl. 85 (2006) 451–464.
[20] J.L. Guermond, J. Oden, S. Prudhomme, Mathematical perspectives on large eddy simulation models for turbulent flows, J. Math. Fluid Mech. 6 (2004) 194–248.
[21] J.L. Guermond, S. Prudhomme, On the construction of suitable solutions to the Navier–Stokes equations and questions regarding the definition of large eddy simulation, Physica D 207 (2005) 64–78.
[22] J.G. Heywood, R. Rannacher, Finite element approximation of the nonstationary Navier–Stokes problem. IV: Error analysis for second-order time discretization, SIAM J. Numer. Anal. 27 (1990) 353–384.
[23] J. Hoffman, C. Johnson, A new approach to computational turbulence modeling, Comput. Methods Appl. Mech. Engrg. 195 (2006) 2865–2880.
[24] T.J.R. Hughes, Multiscale phenomena: Green's function, the Dirichlet-to-Neumann formulation, subgrid scale models, bubbles and the origins of stabilized formulations, Comput. Methods Appl. Mech. Engrg. 127 (1995) 387–401.
[25] T.J.R. Hughes, V.M. Calo, G. Scovazzi, Variational and multiscale methods in turbulence, in: W. Gutkowski, T.A. Kowalewski (Eds.), Proceedings of the XXI international Congress of Theoretical and Applied Mechanics (IUTAM), Kluwer, 2004.
[26] T.J.R. Hughes, G.R. Feijóo, L. Mazzei, J.B. Quincy, The variational multiscale method – a paradigm for computational mechanics, Comput. Methods Appl. Mech. Engrg. 166 (1998) 3–24.
[27] T.J.R. Hughes, L. Mazzei, K.E. Jansen, Large eddy simulation and the variational multiscale method, Comput. Visualiz. Sci. 3 (2000) 47–59.
[28] T.J.R. Hughes, G. Sangalli, Variational multiscale analysis: the fine-scale Green's function, projection, optimization, localization, and stabilized methods, SIAM J. Numer. Anal., to appear.
[29] T.J.R. Hughes, G.N. Wells, Conservation properties for the Galerkin and stabilised forms of the advection–diffusion and incompressible Navier–Stokes equations, Comput. Methods Appl. Mech. Engrg. 194 (2005) 1141–1159.
[30] S. Idelsohn, N. Nigro, M. Storti, G. Buscaglia, A Petrov–Galerkin formulation for advection–reaction–diffusion problems, Comput. Methods Appl. Mech. Engrg. 136 (1996) 27–46.
[31] K.E. Jansen, S.S. Collis, C. Whiting, F. Shakib, A better consistency for low-order stabilized finite element methods, Comput. Methods Appl. Mech. Engrg. 174 (1999) 153–170.
[32] K.E. Jansen, C.H. Whiting, G.M. Hulbert, A generalized-α method for integrating the filtered Navier–Stokes equations with a stabilized finite element method, Comput. Methods Appl. Mech. Engrg. 190 (2000) 305–319.
[33] C. Johnson, U. Nävert, J. Pitkäranta, Finite element methods for linear hyperbolic equations, Comput. Methods Appl. Mech. Engrg. 45 (1984) 285–312.
[34] S.B. Pope, Turbulent Flows, Cambridge University Press, 2000.
[35] P. Sagaut, Large Eddy Simulation for Incompressible Flows, Scientific Computing, Springer, 2001.
[36] F. Shakib, T.J.R. Hughes, A new finite element formulation for computational fluid dynamics: IX. Fourier analysis of space–time Galerkin/least-squares algorithms, Comput. Methods Appl. Mech. Engrg. 87 (1991) 35–58.
[37] R. Temam, Navier–Stokes Equations, North-Holland, 1984.
[38] T. Tezduyar, S. Sathe, Stabilization parameters in SUPG and PSPG formulations, J. Comput. Appl. Mech. 4 (2003) 71–88.